# A thermodynamic model for C-(N-)A-S-H gel: CNASH_ss. Derivation and validation

# A thermodynamic model for C-(N-)A-S-H gel: CNASH_ss. Derivation and validation

**Rupert J. Myers, Susan A. Bernal, John L. Provis ***

Department of Materials Science and Engineering, The University of Sheffield, Sir Robert Hadfield Building, Mappin St, Sheffield S1 3JD, UK

* To whom correspondence should be addressed. Email j.provis@sheffield.ac.uk, phone +44 114 222 5490, fax +44 114 222 5493

## Abstract

The main reaction product in Ca-rich alkali-activated cements and hybrid Portland cement (PC)-based materials is an calcium (alkali) aluminosilicate hydrate (C-(N-)A-S-H) gel. Thermodynamic models without explicit definitions of structurally-incorporated Al species have been used in numerous past studies to describe this gel, but offer limited ability to simulate the chemistry of blended PC materials and alkali-activated cements. Here, a thermodynamic model for C-(N-)A-S-H gel is derived and parameterised to describe solubility data for the CaO-($Na_2O$,$Al_2O_3$)-$SiO_2$-$H_2O$ systems and alkali-activated slag (AAS) cements, and to chemical composition data for C-A-S-H gels. Simulated C-(N-)A-S-H gel densities and molar volumes are consistent with the corresponding values reported for AAS cements, meaning that the model can be used to describe chemical shrinkage in

these materials. Therefore, this model can provide insight into the chemistry of AAS cements at advanced ages, which is important for understanding the long-term durability of these materials.


## Keywords

*B. Calcium-Silicate-Hydrate (C-S-H); B. Thermodynamic Calculations; D. Alkali Activated Cement; D. Blended Cement; E. Modelling.*


## Nomenclature

| | |
|---|---|
| $a$ | Extent of substitution of trivalent cation *R* in bridging sites |
| $\dot{a}$ | Ion size parameter in the extended Debye-Hückel equation (Å) |
| $a'$, $b'$, ..., $e'$ | Stoichiometric coefficients in the additivity method |
| $A_\gamma$ | Temperature-dependent electrostatic parameter in the extended Debye-Hückel equation |
| $BCI$ | Combined $BT$, $CB$ and $IC$ sites ($BCI = BT + CB + IC$) |
| $b^{sc}$ | Neutron scattering length (m) |
| $BT$ | Bridging tetrahedra |
| $B_\gamma$ | Pressure-dependent electrostatic parameter in the extended Debye-Hückel equation |
| $b_\gamma$ | Short-range interaction parameter in the extended Debye-Hückel equation, kg·mol$^{-1}$ |
| $c$ | Charge of the charge-balancing interlayer cation |
| $CB$ | Interlayer charge-balancing species for bridging tetrahedra |
| $CL$ | Chain length of an end-member in the sublattice solid solution model |
| $Cp^o$ | Absolute isobaric heat capacity at standard state (J·mol$^{-1}$·K$^{-1}$) |
| $CU$ | Interstitial 'solid solution' $Ca(OH)_2$ |
| $d_1$, $d_2$ | Coefficients for the $CB$ sites |
| $e_1$, $e_2$ | Coefficients for the $IC$ sites |
| $\Delta_f G^o$ | Standard Gibbs free energy of formation (J·mol$^{-1}$) |
| $G_m$ | Gibbs free energy of mixing (J·mol$^{-1}$) |
| $G_m^E$ | Excess Gibbs free energy of mixing (J·mol$^{-1}$) |
| $h$ | The amount of water per dreierketten unit in a tobermorite-like structure |
| $\Delta_f H^o$ | Standard enthalpy of formation (J·mol$^{-1}$) |
| $i$ | Species of the sublattice solid solution model |

| | |
|---|---|
| $I$ | Ionic strength of the aqueous electrolyte phase in the extended Debye-Hückel equation, mol·kg$^{-1}$ |
| I, II, III, IV, V, VI | Stoichiometric coefficients of the sublattice sites in the solid solution model |
| $i_1 i_2 i_3 \ldots i_s$ | End-member of the sublattice solid solution model written in terms of the species substituted in sublattice sites 1, 2, 3,…, $s$ |
| $IC$ | Interlayer charge-balancing species for the $TU$ sites |
| $IW$ | Interlayer water |
| $k$ | End-member of the sublattice solid solution model |
| $K_{so}$ | Solubility product |
| $l$ | Charge-balancing interlayer cation |
| $MW$ | Molecular weight (g·mol$^{-1}$) |
| $N_A$ | Avogadro constant (6.022 x 10$^{23}$ mol$^{-1}$) |
| $n_s$ | Sublattice sites |
| $R$ | Trivalent cation in tetrahedral coordination |
| $R^*$ | Universal gas constant (8.3145 J·mol$^{-1}$·K$^{-1}$) |
| $s$ | Index of sublattice site $n$ |
| $S^o$ | Absolute entropy at standard state (J·mol$^{-1}$·K$^{-1}$) |
| $T$ | Temperature (K) |
| $TU$ | Main chain site, $CaSiO_{3.5}^-$ |
| $u$ | Interlayer $H^+$ content per dreierketten unit for the $TU$ sites |
| $U$ | Term containing the Gibbs free energies for the reciprocal reactions (J·mol$^{-1}$) |
| $V^o$ | Standard molar volume (J·bar$^{-1}$) |
| $x_{jw}$ | Molar quantity of water in the extended Debye-Hückel equation, mol |
| $X_w$ | Total molar amount of the aqueous phase in the extended Debye-Hückel equation, mol |
| $y_i^{ns}$ | Site fraction of species $i$ in the sublattice site $n_s$ |
| $z_j$ | Charge of aqueous species $j$ |
| $\alpha_k$ | Activity of end-member $k$ |
| $\gamma_j$ | Activity coefficient of aqueous species $j$ |
| $\Delta_{rcp}{}^oG$ | Standard Gibbs free energy of a reciprocal reaction between end-members of the sublattice solid solution model |
| $\zeta$ | Stoichiometric coefficient of the $s^{th}$ sublattice site |
| $\lambda_k$ | Fictive activity coefficient of end-member $k$ |
| $\mu$ | Chemical potential (J·mol$^{-1}$) |
| $v$ | Fraction of bridging site vacancies per dreierketten unit |
| $\rho'$ | Density of an end-member of the sublattice solid solution model (g·m$^{-3}$) |
| $\rho^{sc}$ | Neutron scattering length density (m$^{-2}$) |
| $\Phi^o$ | Standard thermodynamic property estimated by the additivity method |
| $\chi_k^{i,ns}$ | Effective mole fraction of end-member $k$ containing species $i$ in sublattice site $n_s$ |

# 1. Introduction

A key factor governing the long-term performance of any cement or concrete is the stability of the reaction products constituting the solid binder. Work in this area has historically been targeted at understanding the chemistry of the primary reaction product in Portland cement (PC) materials, which is a Ca-rich (Ca/Si > 1.5) calcium silicate hydrate (C-S-H)[a] gel [1]. A substantial amount of this research has been devoted to understanding the solubility of C-S-H gel [2-16], and development of thermodynamic models for this phase has been ongoing over the past decades [15, 17-22]. The Kulik and Kersten C-S-H thermodynamic model [17] has been applied extensively to successfully predict hydrated PC solid phase assemblages and pore solution compositions as a function of the bulk solid binder chemistry [23, 24]. The majority of published solubility data for C-S-H gel have been identified to fall onto several distinct solubility curves [8, 16], indicating that an important and complex structure-solubility relationship exists for this phase. More recently, a structurally-consistent C-S-H thermodynamic model has been developed [25], which has further improved the utility of the thermodynamic modelling approach in understanding the chemistry of PC materials.

Although the chemistry of hydrated neat PC materials is now relatively well established, many modern cements are comprised of blends of PC with Al-containing supplementary cementitious materials (SCMs), which react to form calcium aluminosilicate hydrate (C-A-S-H) gels with significantly lower Ca content (Ca/Si ≤ 1.5) [26, 27]. The level of Ca in the gel is reduced even further in alkali-activated slag (AAS) cements, which are formed through the reaction between ground granulated blast furnace slag (GBFS) and a highly alkaline solution (which are most often Na-based, although the products of activation with alternative alkalis such as K are generally similar [28]). The compositions of the C-A-S-H type gels formed in these cements (denoted C-(N-)A-S-H to reflect the

[a] Cement chemistry shorthand notation is used throughout the text: A, $Al_2O_3$; C, CaO; S, $SiO_2$; H, $H_2O$; and N, $Na_2O$.

63 increased alkali content in addition to the high levels of Al incorporated into this phase) vary
64 depending on the activation conditions, but are typically close to Ca/Si = 1 [29].
65
66 Previous thermodynamic studies of PC/SCM blended cements [26, 30] and AAS cements [31] have
67 utilised empirical descriptions of Al substitution in C-A-S-H and C-(N-)A-S-H gels (e.g. by attributing
68 amounts of Al to these gels to match experimentally measured Al/Si values of the solid binders in
69 the materials), or have neglected to account for the uptake of Al into these phases in the modelling
70 performed, because existing C-S-H thermodynamic model formulations do not contain explicit
71 definitions of Al [15, 17, 18, 21, 25]. The ability to formally account for the extent of Al incorporation
72 into these models is important because it offers scope to significantly improve the level of detail and
73 confidence in predictions of the solid phases formed in the $CaO$-$Al_2O_3$-$SiO_2$-$H_2O$ system as simulated
74 by thermodynamic modelling. Hence, the development of thermodynamic models with explicit
75 descriptions of Al in C-A-S-H and C-(N-)A-S-H gels signifies an important advancement in how
76 cementitious materials are modelled and understood.
77
78 Here, a thermodynamic model is proposed to account explicitly for the tetrahedral Al and Na species
79 bound in C-(N-)A-S-H gel, and applied to simulate the chemistry of AAS cements as an initial
80 example. This model may also be applicable to high-volume blended PC/SCM materials (e.g. CEM III
81 blast furnace cements specified under the EN 197-1 standard) because the structurally-bound Al and
82 alkali species are specified independently in the model formulation, and because the C-(N-)A-S-H
83 and C-A-S-H gels formed in these materials and in AAS cements are similar in nanostructure and
84 chemical composition [26].
85
86
87 ## 2. The chemistry of AAS cements
88

C-(N-)A-S-H gel, which is the dominant reaction product in AAS cements, contains aluminosilicate chains arranged similarly to the disordered tobermorite-like phase C-S-H(I) [1], flanked on either side by an 'interlayer' comprised of $H_2O$ and aqueous cations (e.g. $Ca^{2+}$), and a Ca-O sheet (Figure 1). These aluminosilicate chains are comprised of substituted 'dreierketten' units, which are repeating sets of three silicate tetrahedra (Figure 1). C-(N-)A-S-H gel is believed to exclude Al-O-Al bonding [32], and to only contain significant Al substitution in the bridging tetrahedral sites defined in Figure 1, not in the paired sites [33]. The mean chain length (MCL) is defined here as the number of silicate and aluminate tetrahedra per C-(N-)A-S-H chain. MCL values for C-(N-)A-S-H gels in alkali-activated slag binders with KOH or NaOH activating solutions have been calculated to be between 4 and 8 [34-37] using a non-crosslinked tobermorite/calcium hydroxide representation of this phase [38], compared with 6-11 for C-(N-)A-S-H gels derived from slag reacted with sodium silicate activators [39].

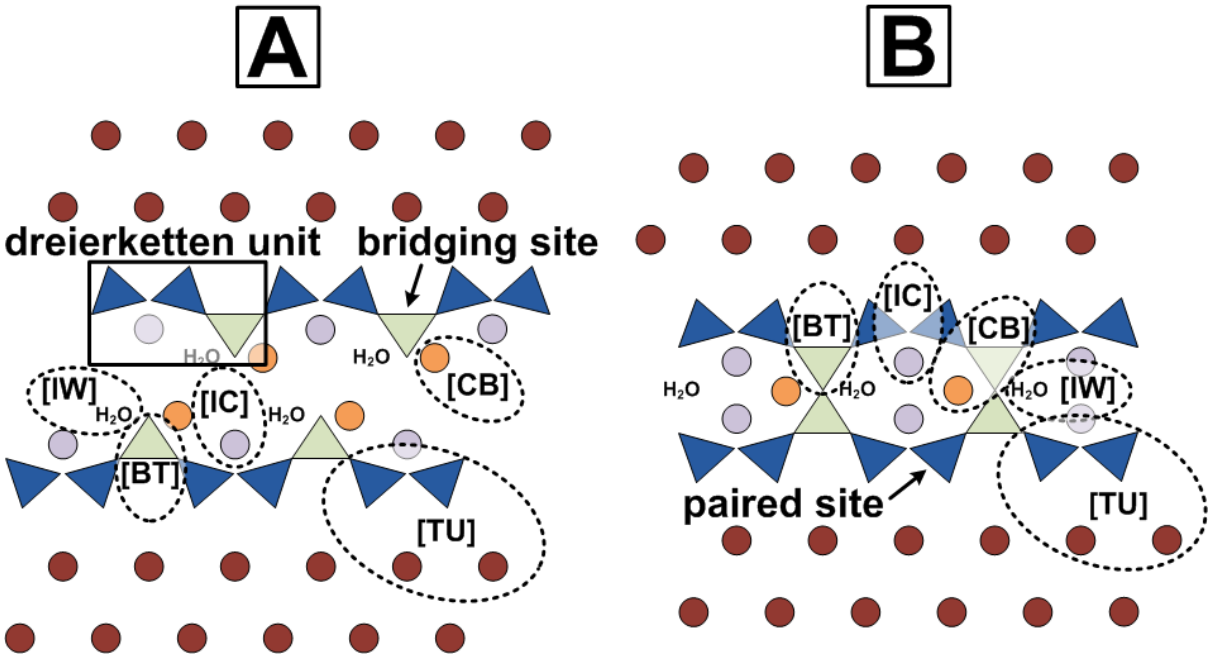


**Figure 1.** Schematic representations of infinite chain length non-crosslinked (A) and crosslinked (B) C-(N-)A-S-H gel structures, with sublattice sites labelled: *TU*; *BT*; *CB*; *IC*; *IW*, as defined in the text (eqs.(2,4)). Light green and dark blue triangles are paired and bridging tetrahedral sites respectively, dark red circles represent Ca sites in the Ca-O sheets, and the orange and purple circles are positively

charged species (typically $Ca^{2+}$, $H^+$, $Na^+$ and/or $K^+$) that charge-balance the aluminosilicate tetrahedra in the $BT$ and $TU$ sites respectively.

Recent experimental results support a partially crosslinked structure for the C-(N-)A-S-H gel formed in $Na_2SiO_3$-activated slag binders: $Q^3$ type species have been identified in deconvolutions of $^{29}Si$ magic angle spinning nuclear magnetic resonance (MAS NMR) spectra in silicate-activated slag cements [39, 40] and in laboratory-synthesised gels [41, 42]. A mixed crosslinked/non-crosslinked structural model was also needed to describe the mechanical properties of hydroxide and silicate-activated slag cements [36].

The majority of AAS and related studies have used GBFS with $Al_2O_3$ content ≤ 14 wt.% and NaOH, KOH or $Na_2O{\cdot}mSiO_2{\cdot}xH_2O$ activators. Most studies using NaOH or KOH solutions have reported Mg-free binder compositions of 0.7 ≤ Ca/Si ≤ 1.2 and Al/Si ≤ 0.25 [35, 43-45], whereas those derived from $Na_2O{\cdot}mSiO_2{\cdot}xH_2O$ solutions usually report Mg-free binder compositions of 0.6 ≤ Ca/Si ≤ 1.2, Al/Si ≤ 0.25 [39, 40, 45, 46]. Laboratory-synthesised solids containing approximately phase-pure C-(N-)A-S-H gels have typically shown chemical compositions of 0.5 < Ca/(Al+Si) ≤ 1 and Al/Si ≤ 0.20 [42, 47, 48].

Bound water is present in variable amounts in the interlayer spacing in C-S-H type structures, with $H_2O$/Si ratios between 1.3-1.7 in gels with no adsorbed water [49], and must also be taken into account in development of thermodynamic models for C-(N-)A-S-H gels. The amount of structurally bound water in AAS cement is variable and not yet fully understood [50], so the water contents of 14Å and 11Å tobermorites may also be used to guide the development of thermodynamic models for C-(N-)A-S-H gels. These minerals have bound $H_2O$/Si ratios of 1.17 and 0.83 respectively [51, 52].

# 3. Sublattice solid solution model for C-(N-)A-S-H gel

## 3.1 Sublattice solid solution definition

There exist several structural models that can describe C-S-H gels, as reviewed in detail by Richardson [53, 54]. However, only the 'Substituted General Model' (SGM) [38] and the 'Crosslinked Substituted Tobermorite Model' (CSTM) [39], can explicitly account for Al-substituted, alkali charge-balanced structures such as C-(N-)A-S-H gel using a fully flexible formulation of the gel chemistry. The CSTM describes C-(N-)A-S-H gel as a mixture of crosslinked and non-crosslinked tobermorite-like structures, and is therefore more generalised than the SGM for systems containing Ca/Si ≤ 1.5 (i.e., excluding solid solution $Ca(OH)_2$). For Ca/Si ≤ 1.5 the treatments of non-crosslinked C-(N-)A-S-H gel components in the SGM and the CSTM are identical, with structural incorporation of Al and charge-balancing by positively-charged interlayer species such as $Na^+$. These structural models can be used to constrain thermodynamic models because they provide a structurally-consistent basis from which chemical compositions of C-(N-)A-S-H end-members can be determined.

Crosslinked and non-crosslinked C-(N-)A-S-H structures cannot always be distinguished from one another by bulk chemical composition alone, which complicates the ability to differentiate between these two structural types in thermodynamic models for this phase. Therefore, the SGM has been used as a basis from which to derive the chemical composition of the C-(N-)A-S-H gel here explicitly in terms of non-crosslinked structures, without precluding the possibility that the thermodynamic model may also implicitly represent the bulk chemistry of crosslinked C-(N-)A-S-H gels. It is also important to note that the C-S-H gel models derived by Kulik [25] used the 'non-substituted general model' developed by Richardson and Groves [55], which is a simpler model related to the SGM. The notation used by Kulik [25] and Richardson and Groves [38, 55] has been conserved where possible for clarity.

The SGM can be represented in terms of one dreierketten unit by eq.(1) (details of the derivation up to this point are provided in Appendix A):

$$\left[\mathrm{Ca(OH)_2}\right]_{\left(\frac{u+y-2}{2}\right)}\cdot\left[\left(\mathrm{CaSiO_{3.5}}\right)_2^-\right]\cdot\left[\left(\mathrm{Si}_{(1-a)}R_a\mathrm{O}_2\right)_{(1-\nu)}\right]^{a(1-\nu)-}\cdot\left[\left(l^{c+}_{\frac{a}{c}(1-\nu)}\right)\right]^{a(1-\nu)+}\cdot\left[\mathrm{Ca}_{\left(1-\frac{u}{2}\right)}\mathrm{H}_u\right]^{2+}\cdot h\mathrm{H_2O} \quad (1)$$

where $R$ is a trivalent cation in tetrahedral coordination (e.g. $Al^{3+}$), $l$ is a charge-balancing interlayer cation (such as $Na^+$, $Ca^{2+}$ and/or $H^+$) with a positive charge of $c$, $a$ is the extent of $R$ substitution in bridging sites (Figure 1), $\nu$ is the fraction of bridging site vacancies per dreierketten unit, $u$ is the interlayer $H^+$ content per dreierketten unit for the main chain sites ($TU$, $\mathrm{CaSiO_{3.5}^-}$), and $h$ defines the amount of water per dreierketten unit. The SGM explicitly defines Al substitution in bridging sites only, and excludes Al-O-Al bonding, consistent with Loewenstein's rule [32].

Eq.(1) can be equivalently written in sublattice notation as eq.(2):

$$\left[CU\right]_2\cdot\left[TU^-\right]_2\cdot\left[BT^{a(1-\nu)-}\right]_1\cdot\left[CB^{a(1-\nu)+}\right]_1\cdot\left[IC^{2+}\right]_1\cdot\left[IW\right]_h \quad (2)$$

where $CU$ represents interstitial 'solid solution' $Ca(OH)_2$ [55], $BT$ are the bridging tetrahedra ($Si_{(1-a)}R_aO_{2(1-\nu)}^{a(1-\nu)-}$), $CB$ are the interlayer charge-balancing species for the bridging tetrahedra ($l_{a(1-\nu)/c}^{a(1-\nu)+}$), $IC$ are the interlayer charge-balancing species for the $TU$ sites ($Ca_{(1-u/2)}H_u^{2+}$), and $IW$ represents interlayer water ($H_2O$). The $CU$ sites in tobermorite are vacant (there is no interstitial 'solid solution' $Ca(OH)_2$), and are therefore eliminated from the structural definition in eqs.(1-2). This limits the chemical composition of the sublattice solid solution model to $0.67 \leq Ca/Si \leq 1.5$ and leads to eqs.(3-4):

$$\left[\left(\mathrm{CaSiO_{3.5}}\right)_2^-\right]\cdot\left[\left(\mathrm{Si}_{(1-a)}R_a\mathrm{O}_2\right)_{(1-\nu)}\right]^{a(1-\nu)-}\cdot\left[\left(l^{c+}_{\frac{a}{c}(1-\nu)}\right)\right]^{a(1-\nu)+}\cdot\left[\mathrm{Ca}_{\left(1-\frac{u}{2}\right)}\mathrm{H}_u\right]^{2+}\cdot h\mathrm{H_2O} \quad (3)$$

$$\left[TU^{-}\right]_2 \cdot \left[BT^{a(1-\nu)-}\right]_1 \cdot \left[CB^{a(1-\nu)+}\right]_1 \cdot \left[IC^{2+}\right]_1 \cdot \left[IW\right]_h \quad (4)$$

This elimination of $Ca(OH)_2$ therefore provides the major limitation on the domain of applicability of the model described here; it is not able to be used for Ca/Si ratios > 1.5, but is valuable for alkali-activated cements and blended PC/SCM materials in which the composition of the C-(N-)A-S-H gel formed falls below this ratio. The sublattice sites shown in eq.(4) are illustrated in Figure 1.

The $IC$ sites are now modified to enable the $TU$ sites to be charge-balanced by $Na^+$ species in addition to the $BT$ sites. The possible interlayer charge-balancing species in C-(N-)A-S-H gel are not limited to $Ca^{2+}$, $H^+$ and $Na^+$, but these are the only species for which sufficient data have been published to enable validation of the thermodynamic model developed here. Na-based solutions are also the most relevant alkaline activators for commercial use because they are relatively inexpensive and widely available [29]. The $BT$ sites in C-(N-)A-S-H gel are mostly filled by vacancies, Si and/or Al species, meaning that $R$ = Al can also be specified. Eq.(3) is re-written with the modified $IC$ sites and with similarly modified $CB$ sites, and with Al-substitution in the $BT$ sites, which results in eq.(5):

$$\left[\left(\mathrm{CaSiO_{3.5}}\right)_2^-\right] \cdot \left[\left(\mathrm{Si_{(1-a)}Al_aO_2}\right)_{(1-\nu)}\right]^{a(1-\nu)-} \cdot \left[\left(\mathrm{Ca_{\left(\frac{1-d_1-d_2}{2}\right)}H_{d_1}Na_{d_2}}\right)_{a(1-\nu)}\right]^{a(1-\nu)+} \cdot \left[\mathrm{Ca_{\left(\frac{2-e_1-e_2}{2}\right)}H_{e_1}Na_{e_2}}\right]^{2+} \cdot h\mathrm{H_2O} \quad (5)$$

where $d_1 + d_2 \leq 1$ and $e_1 + e_2 \leq 2$.

While eqs.(4-5) are satisfactory for thermodynamic modelling, it is desirable to obtain a thermodynamic model which is consistent with existing validated formulations such as the downscaled CSH3T model [25]. In that model, the $BT$, $CB$ and $IC$ sites are combined into two potentially-equivalent $BCI$ sites that could have different substitutions via the choice of two sublattice species, and the sublattice formula was 'downscaled' to 0.5 dreierketten units. The use of two such sites, rather than a single $BCI$ site, is beneficial because it increases the number of unique chemical compositions that can be represented by the sublattice solid solution and can greatly

improve the fit of the thermodynamic model output to the validation data (e.g. solubility measurements) for the same set of mixing rules used (e.g. simple random ideal mixing). However, this means that end-member stoichiometries, and sublattice species and formulae are more likely to be represented in terms of fractional quantities rather than integer amounts. Fractional expressions obviously cannot directly correspond to atomistic-level structures, which means that thermodynamic models developed in this way can only describe the chemistry of solid solutions on the bulk scale rather than at the atomistic scale. Therefore, downscaling is useful in the development of thermodynamic models to describe complex phases such as C-(N-)A-S-H gels with atomistic structures that have not yet been fully resolved. Here, downscaling is essential to improve the number of unique chemical compositions and the volume of experimental data described by the sublattice solid solution model while keeping its formulation relatively simple, particularly because this model is required to describe C-(N-)A-S-H gel chemistry in the complex AAS cement system. The downscaled chemical and sublattice formulae (to 0.5 dreierketten units), written in terms of potentially-equivalent $BCI$ sites ($BCI = BT + CB + IC$) and thus consistent with the downscaled CSH3T model [25], are shown in eqs.(6-7) respectively:

$$\left[\mathrm{CaSiO_{3.5}}\right]^{-} \cdot \left[ \left\{ \left(\mathrm{Si}_{(1-a)}\mathrm{Al}_{a}\mathrm{O}_{2}\right)_{\frac{(1-\nu)}{2}} \cdot \left(\mathrm{Ca}_{\left(\frac{1-d_1-d_2}{2}\right)}\mathrm{H}_{d_1}\mathrm{Na}_{d_2}\right)_{\frac{a(1-\nu)}{2}} \cdot \left(\mathrm{Ca}_{\left(\frac{2-e_1-e_2}{2}\right)}\mathrm{H}_{e_1}\mathrm{Na}_{e_2}\right)_{\frac{1}{2}} \right\}_{\frac{1}{2}}^{0.5+} \right]_{2} \cdot \left[\left(\frac{h}{2}\right)\mathrm{H_2O}\right] \quad (6)$$

$$\left[TU^{-}\right]_{1} \cdot \left[BCI^{0.5+}\right]_{1} \cdot \left[BCI^{0.5+}\right]_{1} \cdot \left[IW\right]_{\frac{h}{2}} \quad (7)$$

Here, at least one additional (Al,Na)-containing sublattice species is necessary to represent C-(N-)A-S-H gel chemistry, compared to previous thermodynamic models for the $CaO$-$SiO_2$-$H_2O$ system. Increasing the number of sublattice species and sites allows the description of a greater diversity of bulk C-(N-)A-S-H gel chemical compositions, and facilitates independent incorporation of Na and Al in C-S-H type structures. Additionally, as the quantities of bound water in C-(N-)A-S-H and C-S-H gels

are significantly different [50, 56], it is also necessary to allow for variation in the $IW$ site. Here, C-(N-)A-S-H gels are assumed to contain one mole of $H_2O$ in the $IW$ site per 0.5 dreierketten units ($h$ = 2), because this is approximately equal to the chemistry of 11 Å and 14 Å tobermorites [51, 52] and the C-A-S-H type gels formed in AAS binders ($H_2O/Si \approx 1$) [50].

These factors thus require the use of a sixth-order sublattice solid solution for the C-(N-)A-S-H thermodynamic model developed here. This solid solution contains five $BCI$ sites, with each carrying a positive charge of 0.125 and grouped as shown in eqs.(8-9), and one variable $IW$ site:

$$\left[\mathrm{CaSiO_{3.5}}\right]^{-}\cdot\left[\mathrm{H_2O}\right]\cdot\left[\left\{\left(\mathrm{Si_{(1-a)}Al_aO_2}\right)_{\frac{(1-\nu)}{2}}\cdot\left(\mathrm{Ca_{\left(\frac{1-d_1-d_2}{2}\right)}H_{d_1}Na_{d_2}}\right)_{\frac{a(1-\nu)}{2}}\cdot\left(\mathrm{Ca_{\left(\frac{2-e_1-e_2}{2}\right)}H_{e_1}Na_{e_2}}\right)_{\frac{1}{2}}\right\}_{\frac{1}{8}}^{0.125+}\right]_8\cdot\left[\left(\frac{h}{2}-1\right)\mathrm{H_2O}\right] \quad (8)$$

$$\left[TU^{-}\right]_1\cdot\left[IW^{*}\right]_1\cdot\left[BCI^{0.125+}\right]_2\cdot\left[BCI^{0.125+}\right]_2\cdot\left[BCI^{0.125+}\right]_2\cdot\left[BCI^{0.125+}\right]_1\cdot\left[BCI^{0.125+}\right]_1\cdot\left[IW\right]_1 \quad (9)$$

where $IW$* represents a fixed interlayer water site (with full occupancy of $H_2O$ but otherwise identical to the $IW$ site depicted in Figure 1). Eqs.(8-9) are the fundamental formulae that represent the C-(N-)A-S-H thermodynamic model developed here.

## 3.2 End-member selection

As discussed in section 1, a goal of this study is to develop a sublattice solid solution model that can describe the solubility and chemical composition of C-(N-)A-S-H gel in AAS cements. Based on the sublattice solid solution definition established in eqs.(8-9), it is now necessary to select a set of end-members, sublattice sites and species that can represent the chemistry of C-(N-)A-S-H gel.

Six species that can substitute into the five *BCI* sites given in eq.(9), and which are compatible with the chemical formula for these sites (eq.(8)) and the chemistry of C-(N-)A-S-H gels in AAS cements, were selected to represent a sublattice solid solution of the form shown in eq.(10):

$$Q^{*}\left[A,B,C,D,E\right]_{\mathrm{I}}^{n_1}\left[F,G,H,I,J\right]_{\mathrm{II}}^{n_2}\left[K,L,M\right]_{\mathrm{III}}^{n_3}\left[N,O,P,Q,R,S\right]_{\mathrm{IV}}^{n_4}\left[T,U,V,W\right]_{\mathrm{V}}^{n_5}\left[X,Y\right]_{\mathrm{VI}}^{n_6} \quad (10)$$

Here, species $A$,$F$,$K$,$N$,$T$ are $Ca_{0.0625}O_{0.0625}H_{0.125}^{0.125+}$, $B$,$G$,$L$,$O$,$U$ are $Si_{0.0625}O_{0.125}H_{0.125}^{0.125+}$ and $D$,$I$,$M$,$Q$,$V$ are $Si_{0.0625}O_{0.125}Na_{0.125}^{0.125+}$, which can be present in five different *BCI* sites, the species $C$,$H$,$P$ are $Al_{0.0625}O_{0.125}H_{0.1875}^{0.125+}$ and $E$,$J$,$R$ are $Al_{0.0625}Na_{0.0625}O_{0.125}H_{0.125}^{0.125+}$, which can fill four of the *BCI* sites, the species $S$,$W$ are $Ca_{0.0625}O_{0.0625}Na_{0.125}^{0.125+}$, which can fill two of the *BCI* sites, $X$ is $H_2O$, $Y$ is a vacancy ($V_{IW}$), and $Q^{*}$ is $CaSiO_{3.5}^{-}\cdot H_2O$. This combination of sublattice sites and species was chosen as it comprises the least complex formulation of the sublattice solid solution that can represent the chemistry of the C-(N-)A-S-H gel in AAS cements. In this work the coefficients $\mathrm{I}=2$, $\mathrm{II}=2$, $\mathrm{III}=2$, $\mathrm{IV}=1$, $\mathrm{V}=1$ and $\mathrm{VI}=1$ define the stoichiometry of the sublattice sites, and the superscripts $n_1$, $n_2$, $n_3$, $n_4$, $n_5$ and $n_6$ correspond to the five *BCI* sites and single *IW* site in eq.(9). Vacancies in *BCI* sites are included in the thermodynamic model via the $v$ parameter in eq.(8).

A minimal set of eight end-members was chosen within this sublattice solid solution model to define the C-(N-)A-S-H gel in this work, as shown in Table 1. This is the smallest number of end-members that can resemble the chemistry of C-(N-)A-S-H gels (section 2) and describe the available solubility data for AAS cement and the CaO-($Na_2O$,$Al_2O_3$)-$SiO_2$-$H_2O$ systems (section 6). The solid solution contains three C-S-H end-members, one C-(N-)S-H end-member, two C-A-S-H end-members and two C-(N-)A-S-H end-members. The C-S-H end-members have the same chemical compositions as the T2C, T5C and TobH end-members of the downscaled CSH3T model (T2C*, T5C* and TobH* respectively) [25], which contain the *TU* site, $h = 4$, and two *BCI* sublattice species, $Si_{0.25}O_{0.5}H_{0.5}^{+}$ and $Ca_{0.25}O_{0.25}H_{0.5}^{+}$, for $a = 0$, to cover the range 0.67 ≤ Ca/Si ≤ 1.5 in the CaO-$SiO_2$-$H_2O$ system. One

278 $H_2O$ molecule is also added per vacancy in the bridging tetrahedra for each of the eight end-
279 members (determined by the value of $v$).
280

**Table 1**. Chemical compositions of the eight end-members of the C-(N-)A-S-H thermodynamic model, and parameters chosen for use in eq.(8). One $H_2O$ molecule is added to the *BCI* site per bridging site vacancy for consistency with the C-S-H thermodynamic model developed by Kulik [25].

| End-member | $v$ | $a$ | $i_1$ | $i_2$ | $u_1$ | $u_2$ | $M$ | Sublattice formula [b] | Chemical formula |
|---|---|---|---|---|---|---|---|---|---|
| 5CA | 0.5 | 1 | 1 | 0 | 1 | 0 | 2 | $[(CaSiO_{3.5})^-]_1{\cdot}[H_2O]_1{\cdot}[Al_{0.0625}O_{0.125}H_{0.1875}{}^{0.125+}]_2{\cdot}$ $[Al_{0.0625}O_{0.125}H_{0.1875}{}^{0.125+}]_2{\cdot}[Ca_{0.0625}O_{0.0625}H_{0.125}{}^{0.125+}]_2{\cdot}$ $[Ca_{0.0625}O_{0.0625}H_{0.125}{}^{0.125+}]_1{\cdot}[Ca_{0.0625}O_{0.0625}H_{0.125}{}^{0.125+}]_1{\cdot}[V_{H2O}]_1$ | $(CaO)_{1.25}(Al_2O_3)_{0.125}(SiO_2)_1(H_2O)_{1.625}$ |
| INFCA | 0 | 0.625 | 1 | 0 | 2 | 0 | 2 | $[(CaSiO_{3.5})^-]_1{\cdot}[H_2O]_1{\cdot}[Al_{0.0625}O_{0.125}H_{0.1875}{}^{0.125+}]_2{\cdot}$ $[Al_{0.0625}O_{0.125}H_{0.1875}{}^{0.125+}]_2{\cdot}[Si_{0.0625}O_{0.125}H_{0.125}{}^{0.125+}]_2{\cdot}$ $[Al_{0.0625}O_{0.125}H_{0.1875}{}^{0.125+}]_1{\cdot}[Si_{0.0625}O_{0.125}H_{0.125}{}^{0.125+}]_1{\cdot}[V_{H2O}]_1$ | $(CaO)_1(Al_2O_3)_{0.15625}(SiO_2)_{1.1875}(H_2O)_{1.65625}$ |
| 5CNA | 0.5 | 1 | 0 | 1 | 0.5 | 0.5 | 2 | $[(CaSiO_{3.5})^-]_1{\cdot}[H_2O]_1{\cdot}[Al_{0.0625}Na_{0.0625}O_{0.125}H_{0.125}{}^{0.125+}]_2{\cdot}$ $[Al_{0.0625}Na_{0.0625}O_{0.125}H_{0.125}{}^{0.125+}]_2{\cdot}[Ca_{0.0625}O_{0.0625}H_{0.125}{}^{0.125+}]_2{\cdot}$ $[Ca_{0.0625}O_{0.0625}Na_{0.125}{}^{0.125+}]_1{\cdot}[Ca_{0.0625}O_{0.0625}Na_{0.125}{}^{0.125+}]_1{\cdot}[V_{H2O}]_1$ | $(CaO)_{1.25}(Na_2O)_{0.25}(Al_2O_3)_{0.125}(SiO_2)_1(H_2O)_{1.375}$ |
| INFCNA | 0 | 0.625 | 0 | 1 | 1.25 | 0.75 | 2 | $[(CaSiO_{3.5})^-]_1{\cdot}[H_2O]_1{\cdot}[Al_{0.0625}Na_{0.0625}O_{0.125}H_{0.125}{}^{0.125+}]_2{\cdot}$ $[Al_{0.0625}Na_{0.0625}O_{0.125}H_{0.125}{}^{0.125+}]_2{\cdot}[Si_{0.0625}O_{0.125}Na_{0.125}{}^{0.125+}]_2{\cdot}$ $[Al_{0.0625}Na_{0.0625}O_{0.125}H_{0.125}{}^{0.125+}]_1{\cdot}[Si_{0.0625}O_{0.125}Na_{0.125}{}^{0.125+}]_1{\cdot}[V_{H2O}]_1$ | $(CaO)_1(Na_2O)_{0.34375}(Al_2O_3)_{0.15625}(SiO_2)_{1.1875}(H_2O)_{1.3125}$ |
| INFCN | 0 | 0 | 1 | 0 | 0.75 | 1.25 | 2 | $[(CaSiO_{3.5})^-]_1{\cdot}[H_2O]_1{\cdot}[Si_{0.0625}O_{0.125}Na_{0.125}{}^{0.125+}]_2{\cdot}$ $[Si_{0.0625}O_{0.125}Na_{0.125}{}^{0.125+}]_2{\cdot}[Si_{0.0625}O_{0.125}H_{0.125}{}^{0.125+}]_2{\cdot}$ $[Si_{0.0625}O_{0.125}Na_{0.125}{}^{0.125+}]_1{\cdot}[Si_{0.0625}O_{0.125}H_{0.125}{}^{0.125+}]_1{\cdot}[V_{H2O}]_1$ | $(CaO)_1(Na_2O)_{0.3125}(SiO_2)_{1.5}(H_2O)_{1.1875}$ |
| T2C* [a] | 1 | 0 | 0 | 0 | 0 | 0 | 4 | $[(CaSiO_{3.5})^-]_1{\cdot}[H_2O]_1{\cdot}[Ca_{0.0625}O_{0.0625}H_{0.125}{}^{0.125+}]_2{\cdot}$ $[Ca_{0.0625}O_{0.0625}H_{0.125}{}^{0.125+}]_2{\cdot}[Ca_{0.0625}O_{0.0625}H_{0.125}{}^{0.125+}]_2{\cdot}$ $[Ca_{0.0625}O_{0.0625}H_{0.125}{}^{0.125+}]_1{\cdot}[Ca_{0.0625}O_{0.0625}H_{0.125}{}^{0.125+}]_1{\cdot}[H_2O]_1$ | $(CaO)_{1.5}(SiO_2)_1(H_2O)_{2.5}$ |
| T5C* [a] | 0.5 | 0 | 0 | 0 | 1 | 0 | 4 | $[(CaSiO_{3.5})^-]_1{\cdot}[H_2O]_1{\cdot}[Si_{0.0625}O_{0.125}H_{0.125}{}^{0.125+}]_2{\cdot}$ $[Si_{0.0625}O_{0.125}H_{0.125}{}^{0.125+}]_2{\cdot}[Ca_{0.0625}O_{0.0625}H_{0.125}{}^{0.125+}]_2{\cdot}$ $[Ca_{0.0625}O_{0.0625}H_{0.125}{}^{0.125+}]_1{\cdot}[Ca_{0.0625}O_{0.0625}H_{0.125}{}^{0.125+}]_1{\cdot}[H_2O]_1$ | $(CaO)_{1.25}(SiO_2)_{1.25}(H_2O)_{2.5}$ |
| TobH* [a] | 0 | 0 | 0 | 0 | 2 | 0 | 4 | $[(CaSiO_{3.5})^-]_1{\cdot}[H_2O]_1{\cdot}[Si_{0.0625}O_{0.125}H_{0.125}{}^{0.125+}]_2{\cdot}$ $[Si_{0.0625}O_{0.125}H_{0.125}{}^{0.125+}]_2{\cdot}[Si_{0.0625}O_{0.125}H_{0.125}{}^{0.125+}]_2{\cdot}$ $[Si_{0.0625}O_{0.125}H_{0.125}{}^{0.125+}]_1{\cdot}[Si_{0.0625}O_{0.125}H_{0.125}{}^{0.125+}]_1{\cdot}[H_2O]_1$ | $(CaO)_1(SiO_2)_{1.5}(H_2O)_{2.5}$ |

[a] The asterisks for the T2C*, T5C* and TobH* end-members indicate that these components have the same bulk chemistry but slightly modified thermodynamic properties relative to the T2C, T5C and TobH end-members of the downscaled CSH3T model [25].

[b] $V_{H2O}$ is a vacancy in the *IW* sublattice site.

As each species ($A$ to $Y$) is defined to only substitute into one site (i.e., species with the same chemistry but occupying different sites are treated as being distinct), the site fraction of a species $i$ in a given site $n_s$, $y_i^{n_s}$, is defined as $y_i^{n_s} = \sum\left(\chi_k^{i,n_s}\right)$ for $\sum\left(y_i^{n_s}\right) = 1$. Here $n_s \in \{n_1, n_2, n_3, n_4, n_5, n_6\}$ is the sublattice site, $\chi_k^{i,n_s}$ is the effective mole fraction of end-member $k$ containing the species $i$ in the sublattice site $n_s$, with $\sum_k(\chi_k) = 1$. In defining an end-member of the sublattice solid solution model, the species present in the $s^{th}$ sublattice site may be identified by the same subscript number i.e. $i_1$ is the species present in the sublattice site $n_1$, and $i_1 \in \{A, B, C, D, E\}$. Thus an end-member can be equivalently written in terms of its substituting species, i.e. $k = i_1 i_2 i_3 \cdots i_s$.

The chain length ($CL$) for each of the end-members, and the MCL of the C-(N-)A-S-H gel as a whole, can then be calculated from eq.(11).

$$CL = \frac{3}{\sum_k(\chi_k \nu_k)} - 1 \tag{11}$$

The fraction of bridging site vacancies per dreierketten unit, $v$, is shown in Table 1 for each end-member of the C-(N-)A-S-H thermodynamic model. This equation represents the minimum chain length possible for the end-members, and thus the minimum MCL of the C-(N-)A-S-H gel, because eq.(11) implies that the end-members are strictly non-crosslinked. The chain lengths of crosslinked C-(N-)A-S-H end-members would be calculated in the same way, but with a factor of two included (i.e. $CL_{crosslinked} = 2CL$) to reflect the double chain structures in these phases. Here, these crosslinked and non-crosslinked structures were not explicitly differentiated in defining the end-members (eqs.(8-9)), meaning that eq.(11) provides a lower bound on the MCLs of partially (or fully) crosslinked C-(N-)A-S-H gels.

# 4. Thermodynamic basis of the sublattice solid solution model

The chemical potential (partial molal Gibbs free energy), $\mu_{i_1 i_2 i_3 \cdots i_s}$, of end-member $i_1 i_2 i_3 \cdots i_s$ in a multi-component solid solution can be represented by eq.(12) [57]:

$$\mu_{i_1 i_2 i_3 \cdots i_s} = G_m + \left[ \frac{\partial G_m}{\partial y_{i_1}^{n_1}} + \frac{\partial G_m}{\partial y_{i_2}^{n_2}} + \frac{\partial G_m}{\partial y_{i_3}^{n_3}} + \cdots + \frac{\partial G_m}{\partial y_{i_s}^{n_s}} \right] - \left[ \sum_i \left( y_i \frac{\partial G_m}{\partial y_i} \right) \right] \tag{12}$$

where $G_m$ is the Gibbs free energy of mixing using the notation previously introduced, and can be expressed by eq.(13) [58]:

$$G_m = G^{mech} - TS_m^{id} + G_m^E \tag{13}$$

where $G^{mech}$ is the Gibbs free energy of a compositionally-equivalent 'mechanical mixture' of simple components to the solid solution phase, $S_m^{id}$ is the difference in entropy between the ideal solid solution for the solid phase and its end-member components (i.e. the configurational entropy), and $G_m^E$ is the excess Gibbs free energy of mixing (representing the deviation of the solid solution from ideality).

Here, the 'compound energy formalism' is used to define the surface of reference for the Gibbs free energy of mixing as a weighted average of the Gibbs free energy of each of the (pure) end-members in the C-(N-)A-S-H solid solution [57]. This is formally expressed by eq.(14) for a multi-site, multi-component sublattice solid solution, assuming random mixing within each sublattice [59]:

$$\begin{aligned} G_m = & \left[ \sum_{n_1} \sum_{n_2} \sum_{n_3} \cdots \sum_{n_s} \left( y_{i_1}^{n_1} y_{i_2}^{n_2} y_{i_3}^{n_3} \cdots y_{i_s}^{n_s} \right) \cdot {}^{o}G_{i_1 i_2 i_3 \cdots i_s} \right] + \\ & R^* T \left[ \mathrm{I} \sum_{i_1} \left( y_{i_1} \ln \left( y_{i_1} \right) \right) + \mathrm{II} \sum_{i_2} \left( y_{i_2} \ln \left( y_{i_2} \right) \right) + \mathrm{III} \sum_{i_3} \left( y_{i_3} \ln \left( y_{i_3} \right) \right) + \cdots + \zeta \sum_{i_s} \left( y_{i_s} \ln \left( y_{i_s} \right) \right) \right] + G_m^E \end{aligned} \tag{14}$$

where ${}^{o}G_{i_1 i_2 i_3 \cdots i_s}$ is the standard Gibbs free energy of end-member $i_1 i_2 i_3 \cdots i_s$, $R^*$ is the universal gas constant, $T$ is temperature and $\zeta$ is the stoichiometric coefficient of the $s^{\text{th}}$ sublattice site. The random mixing assumption is appropriate here because it greatly simplifies the expression for the

configurational entropy and because the solid solution definition (eqs.(8-9)) does not represent atomic-scale structures; assigning hypothetical weightings to non-physical mixing combinations would not make physical sense. This choice is reasonable given that this is the first attempt to develop a sublattice solid solution model for C-(N-)A-S-H gel, and will be validated in section 6 through the ability of the model to accurately describe chemical composition and solubility data for this phase.

Eq.(14) can be expanded explicitly for the sublattice solid solution defined by the eight end-members shown in Table 1. Substituting this expanded version of eq.(14) into eq.(12), defining a generalised end-member with species $A$, $F$, $K$, $N$, $T$, $X$ in sublattice sites $n_1$, $n_2$, $n_3$, $n_4$, $n_5$, $n_6$ and then simplifying, results in eq.(15):

$$\mu_{AFKNTX} = {}^{o}G_{AFKNTX} + R^{*}T\left[2\ln\left(y_A\right)+2\ln\left(y_F\right)+2\ln\left(y_K\right)+\ln\left(y_N\right)+\ln\left(y_T\right)+\ln\left(y_X\right)\right]+G_m^E+U \quad (15)$$

Equivalent relationships for $\mu_{AFKNTX}$ can be written for all other combinations of sublattice site occupancies. The $U$ term contains the Gibbs free energies for the reciprocal reactions ($\Delta_{rcp}{}^{o}G$), which denotes the difference in Gibbs free energy between combinations of end-members in the sublattice solid solution (which must by definition contain equal numbers of reactant and product terms). For example, the reciprocal reaction (eq.(16)) has a corresponding Gibbs free energy of reaction given by eq.(17):

$$AFKOTX + AFLNTX \leftrightarrow AFKNTX + AFLOTX \quad (16)$$

$$\Delta_{rcp}{}^{o}G_{LO} = {}^{o}G_{AFKOTX} + {}^{o}G_{AFLNTX} - {}^{o}G_{AFKNTX} - {}^{o}G_{AFLOTX} \quad (17)$$

It is possible to make two key simplifications here. The first is setting $G_m{}^E$ = 0, i.e. interactions between atoms in the same sublattice sites are neglected, meaning that the sublattice solid solution model is ideal. The second is that the Gibbs free energies of the reciprocal reactions in the solid

356 solution are numerically approximated to zero ($U$ = 0). The reciprocal reaction terms describe the
357 nearest-neighbour interactions in the solid solution, so are likely to influence end-member chemical
358 potentials more than the next-nearest-neighbour interactions described by the excess Gibbs free
359 energy terms. These terms are likely to be non-zero in C-(N-)A-S-H gels, because it is known that
360 thermodynamic energetic differences arise from nearest-neighbour Si-Al substitution in
361 aluminosilicate systems [60], but this approach can be validated by the good fit of the
362 thermodynamic model to the published solubility and chemical composition data in the CaO-
363 ($Na_2O$,$Al_2O_3$)-$SiO_2$-$H_2O$ systems (section 6). In defining the mixing rules in this way, the accuracy of
364 the thermodynamic model is determined semi-empirically through the use of end-members with
365 carefully selected chemical compositions and Gibbs free energies that internalise the nearest and
366 next-nearest neighbour interactions in C-(N-)A-S-H gels, rather than through the explicit definition of
367 these interactions. However, quantification of these interactions in terms of chemical potentials for
368 hypothetical C-(N-)A-S-H end-members, and a better understanding of the solubility of C-(N-)A-S-H
369 gels, will be important future steps in the model development.
370
371 Application of these assumptions to eq.(15) leads to the final, simplified formula for the chemical
372 potential of an end-member in the C-(N-)A-S-H sublattice solid solution model (eq.(18)):

373
$$\mu_{AFKNTX} = {}^{o}G_{AFKNTX} + R^{*}T\left[2\ln\left(y_A\right)+2\ln\left(y_F\right)+2\ln\left(y_K\right)+\ln\left(y_N\right)+\ln\left(y_T\right)+\ln\left(y_X\right)\right] \quad (18)$$

374
375 The C-(N-)A-S-H thermodynamic model developed here is implemented in the GEM-Selektor v3
376 thermodynamic modelling software (http://gems.web.psi.ch/) [61, 62]. Sublattice solid solution
377 models can be specified in GEM-Selektor by modifying the activities of the chosen end-members
378 (Table 1) through the introduction of a 'fictive activity coefficient' $\lambda$, which internalises the
379 thermodynamic mixing relationships within the solid solution. This method was used in the C-S-H
380 thermodynamic model developed by Kulik [25]. The fictive activity coefficient is defined by eq.(19):

$$\lambda_k = \frac{\alpha_k}{\chi_k} \tag{19}$$

where $\alpha_k$ is the activity of the $k^{th}$ end-member, eq.(20):

$$\mu_k = \mu_k^o + R^* T \ln(\alpha_k) \tag{20}$$

The fictive activity coefficient is defined by eliminating $\mu_k$ and the ${}^oG_{AFKNTX}$ term (equivalent to $\mu_k{}^o$ as defined here) from eqs.(18,20), then substituting eq.(19) into the resulting equation and simplifying to obtain eq.(21):

$$\ln(\lambda_{AFKNTX}) = \left[2\ln(y_A) + 2\ln(y_F) + 2\ln(y_K) + \ln(y_N) + \ln(y_T) + \ln(y_X)\right] - \ln(\chi_{AFKNTX}) \tag{21}$$

Relationships equivalent to eq.(21) can thus be obtained for all eight end-members (Table 1). The fictive activity coefficient relationships for these end-members are shown in Appendix B.

# 5. Modelling method

## 5.1 Modelling system definition

The kernel Nagra/PSI [63], which is the default thermodynamic database for GEM-Selektor v3 (http://gems.web.psi.ch/) [61, 62], and the CEMDATA07 thermodynamic database [17, 23, 64-69], which contains data for various compounds commonly found in cement systems, were used during simulations. The ideal gas equation of state is used to describe the gases and the Truesdell-Jones form of the extended Debye-Hückel equation, eq.(22) [70], is used to describe the aqueous species.

$$\log_{10}\gamma_j = \frac{-A_\gamma z_j^2 \sqrt{I}}{1 + \dot{a} B_\gamma \sqrt{I}} + b_\gamma I + \log_{10}\frac{x_{jw}}{X_w} \tag{22}$$

Here, $\gamma_j$ and $z_j$ are the activity coefficient and charge of the $j^{th}$ aqueous species respectively, $A_\gamma$ and $B_\gamma$ are temperature and pressure-dependent electrostatic parameters, $I$ is the ionic strength of the aqueous electrolyte phase, $\dot{a}$ is the ion size parameter, $b_\gamma$ is a parameter that describes short-range interactions between charged aqueous species in an electrolyte solution (representing the predominant electrolyte in the system), $x_{jw}$ is the molar quantity of water, and $X_w$ is the total molar amount of the aqueous phase. Constant values of $\dot{a}$ (3.31 Å) and $b_\gamma$ (0.098 kg/mol) are taken to represent the average ion size and common short-range interactions of charged aqueous species in a NaOH-dominated solution [70]. The water activity is calculated from the osmotic coefficient [70].

The extended Debye-Hückel equation is accurate at moderate ionic strengths (up to ~ 1 molal) [70], which is lower than the ionic strength in AAS pore solutions (~1-3 molal in sodium silicate activated slag cements, e.g. [71]), but this equation was chosen here as a first step in development of the thermodynamic model as it is directly encoded in GEM-Selektor. Additionally, the description of aqueous silicate speciation in the GEM-Selektor databases does not currently extend beyond dimeric silicate and aluminosilicate units, and adsorption of aqueous species onto simulated solid phases is also not fully taken into account. Use of an improved aqueous phase model, such as the Pitzer model [72] coupled with a more complete description of silicate oligomerisation [73], and description of sorption effects, are goals of future work.

## 5.2 Thermodynamic property estimation

The standard absolute isobaric heat capacity ($Cp^o$) and absolute entropy at standard state ($S^o$) of the five (Al,Na)-containing C-(N-)A-S-H end-members were estimated using the additivity method and eq.(23), defined in terms of structurally-relevant constituents: T2C (the Ca-rich end-member of the downscaled CSH3T model [25], $(CaO)_{1.5}(SiO_2)_1(H_2O)_{2.5}$), portlandite ($Ca(OH)_2$), amorphous $SiO_2$, gibbsite ($Al(OH)_3$) and $NaOH_{(s)}$.

$$\Phi^{o}_{(CaO)_{a'}(SiO_2)_{b'}(Al_2O_3)_{c'}(Na_2O)_{d'}(H_2O)_{e'}} = \frac{1}{2}(5a'-3e'+9c'+3d')\Phi^{o}_{Ca(OH)_2} + (b'-e'+a'+3c'+d')\Phi^{o}_{SiO_2} + 2c'\Phi^{o}_{Al(OH)_3} + 2d'\Phi^{o}_{NaOH} + (e'-a'-3c'-d')\Phi^{o}_{(CaO)_{1.5}(SiO_2)_1(H_2O)_{2.5}} \quad (23)$$

Here $\Phi^o$ denotes the standard thermodynamic property undergoing estimation ($Cp^o$ or $S^o$), *a'*, *b'*, *c'*, *d'*, *e'* are the stoichiometric coefficients for the respective oxide components CaO, $SiO_2$, $Al_2O_3$, $Na_2O$ and $H_2O$, and the numerical coefficients for these terms are the values that result from solving the elemental balance for eq.(23). The thermodynamic properties of the constituent phases are provided in Appendix C, and are consistent with the Nagra/PSI [63] and CEMDATA07 thermodynamic databases [17, 23, 64-69]. The additivity method is expected to yield relatively small errors in estimated values for $Cp^o$ and $S^o$ if suitable constituents are chosen [74]. The changes in $S^o$ and $Cp^o$, and the solubility product ($K_{so}$) of the (Al,Na)-containing C-(N-)A-S-H end-members for the dissociation reaction represented by eq.(24), were determined to enable thermodynamic property calculations in GEM-Selektor:

$$(CaO)_{a'}(SiO_2)_{b'}(Al_2O_3)_{c'}(Na_2O)_{d'}(H_2O)_{e'(s)} \xleftrightarrow{K_{so}} a'Ca^{2+}_{(aq)} + b'SiO_3^{2-}{}_{(aq)} + 2c'AlO_2^{-}{}_{(aq)} + 2d'Na^{+}_{(aq)} + 2(a'-b'-c'+d')OH^{-}_{(aq)} + (b'+c'+e'-a'-d')H_2O_{(l)} \quad (24)$$

The ReacDC module in GEM-Selektor was used to determine the standard partial molal Gibbs free energies ($\Delta_f G^o$) and enthalpies of formation ($\Delta_f H^o$) for the proposed C-(N-)A-S-H end-members by specifying 'optimised' solubility products for the reaction shown in eq.(24), the value of $S^o$ determined via the additivity method (using the components listed previously), and the change in $S^o$ of the dissociation reaction (eq.(24)). The Gibbs free energies (and thus the enthalpies) of the T2C*, T5C* and TobH* end-members were modified slightly from the values reported in the downscaled CSH3T model [25], and solubility products of the (Al,Na)-containing C-(N-)A-S-H end-members were

449 selected, to obtain the optimised fit of the thermodynamic model to the solubility and solid phase
450 chemistry data in the CaO-($Na_2O$,$Al_2O_3$)-$SiO_2$-$H_2O$ [2-15, 41, 42, 48, 75-81] and AAS cement systems
451 [71, 82-84] used in model validation (section 6). All other thermodynamic parameters of the T2C*,
452 T5C* and TobH* end-members were adopted directly from the downscaled CSH3T model.
453
454 Standard molar volumes ($V^o$) of the (Al,Na)-containing C-(N-)A-S-H end-members were determined
455 from density calculations using the method proposed by Thomas et al. [50], but extended to include
456 Na species via eq.(25):

457 $$\rho^{sc}{}_{CNASH} = N_A \rho'_{CNASH} \left[ \frac{\left(\frac{CaO}{SiO_2}\right) b^{sc}{}_{CaO} + b^{sc}{}_{SiO_2} + \left(\frac{Al_2O_3}{SiO_2}\right) b^{sc}{}_{Al_2O_3} + \left(\frac{Na_2O}{SiO_2}\right) b^{sc}{}_{Na_2O} + \left(\frac{H_2O}{SiO_2}\right) b^{sc}{}_{H_2O}}{MW_{CNASH}} \right] \quad (25)$$

458 where the $b^{sc}$ parameters are the established neutron scattering lengths for CaO, $SiO_2$, $Al_2O_3$, $Na_2O$
459 and $H_2O$, $\rho^{sc}$ is the scattering length density taken from the literature [50], $\rho'_{CNASH}$ is the predicted
460 density of a C-(N-)A-S-H end-member, $N_A$ is Avogadro's number, $MW_{CNASH}$ is the molecular weight of
461 a C-(N-)A-S-H end-member, and the ratios CaO/$SiO_2$, $Al_2O_3$/$SiO_2$, $Na_2O$/$SiO_2$, and $H_2O$/$SiO_2$ are molar
462 composition ratios of a C-(N-)A-S-H end-member. The optimised thermodynamic properties for the
463 C-(N-)A-S-H end-members are summarised in Table 2.
464
465 **Table 2**. Thermodynamic properties, densities and the change in thermodynamic properties for the
466 dissociation reaction (eq.(24)) for the end-members of the C-(N-)A-S-H solid solution (25°C, 1 bar)

| **Standard thermodynamic properties and density** | | | | | | |
|---|---|---|---|---|---|---|
| **End-member** | $V°$ (cm³/mol) | $\Delta_f H°$ (kJ/mol) | $\Delta_f G°$ (kJ/mol) | $S°$ (J/mol.K) | $Cp°$ (J/mol.K) | $\rho'_{CNASH}$ (g/cm³) |
| 5CA | 57.3 | -2491 | -2293 | 163 | 177 | 3.01 |
| INFCA | 59.3 | -2551 | -2343 | 154 | 181 | 2.92 |
| 5CNA | 64.5 | -2569 | -2382 | 195 | 176 | 2.84 |
| INFCNA | 69.3 | -2667 | -2474 | 198 | 180 | 2.72 |
| INFCN | 71.1 | -2642 | -2452 | 186 | 184 | 2.63 |
| T2C* [a] | 80.6 | -2721 | -2465 | 167 | 237 | 2.35 |
| T5C* [a] | 79.3 | -2780 | -2517 | 160 | 234 | 2.40 |
| TobH* [a] | 85.0 | -2831 | -2560 | 153 | 231 | 2.25 |
| **Change in thermodynamic properties for the dissociation reaction (eq.(24))** | | | | | | |
| **End-member** | $\Delta_r V°$ | $\Delta_r H°$ | $\Delta_r G°$ | $\Delta_r S°$ | $\Delta_r Cp°$ | $\log_{10}(K_{so})$ |

| | ($cm^3$/mol) | (kJ/mol) | (kJ/mol) | (J/mol.K) | (J/mol.K) | |
|---|---|---|---|---|---|---|
| 5CA | -17.9 | -4.0 | 61.4 | -219 | -29.3 | -10.75 |
| INFCA | 5.1 | 0.58 | 50.8 | -168 | 160 | -8.90 |
| 5CNA | -37.1 | -18.8 | 59.4 | -262 | -115 | -10.4 |
| INFCNA | -21.3 | -10.8 | 57.1 | -228 | 41.5 | -10.0 |
| INFCN | -12.5 | -6.2 | 61.1 | -226 | 144 | -10.7 |

[a] The $\log_{10}(K_{so})$ values for the T2C*, T5C* and TobH* end-members, for the dissociation reaction eq.(24), are -11.6, -10.5 and -7.9 respectively.

# 6. Application of the thermodynamic model in GEM-Selektor

## 6.1 Approach

The success of a thermodynamic model is measured in terms of its ability to describe the available thermochemical data in the target system(s) - here, for Ca-rich alkali-activated cements such as AAS cements and hybrid alkali-activated/PC materials - and its ability to predict the chemistry of simulated systems where experimental data are either not available or are difficult to obtain. Hence, thermodynamic models for cements must be developed using existing experimental results such as solubility measurements [8, 47], solid product assemblages [35, 37, 43], and/or the chemistry of C-(N-)A-S-H gels [42]. An extensive set of experimental solubility data in the $CaO$-$SiO_2$-$H_2O$ system is available for the development of thermodynamic models for C-S-H gels [2-15], but the use of such information to develop models for C-(N-)A-S-H gels is significantly more complicated. Solubility measurements in the $CaO$-$Na_2O$-$Al_2O_3$-$SiO_2$-$H_2O$ system are not available in sufficient detail to enable development of thermodynamic models using this information alone, meaning that validation against other data is necessary. In this light, AAS cements provide an opportunity to validate the thermodynamic model; these materials are described mostly in terms of the more complex $CaO$-$Na_2O$-$Al_2O_3$-$SiO_2$-$H_2O$-$MgO$ system, but are relatively well characterised. Hence, the thermodynamic model here is validated for the less complex $CaO$-($Na_2O$,$Al_2O_3$)-$SiO_2$-$H_2O$ systems, and also AAS

cements. The ability of the thermodynamic model to predict solid phase assemblages in these systems will be discussed in a subsequent publication.

GEM-Selektor simulations for the $CaO$-$SiO_2$-$H_2O$ and $CaO$-($Na_2O$,$Al_2O_3$)-$SiO_2$-$H_2O$ systems were performed at a constant temperature and pressure of 25°C and 1 bar, using 1 g of each of the gases $O_{2\,(g)}$ and $N_{2\,(g)}$. Simulations were performed by adding $H_2O$, NaOH, CaO, $Al(OH)_3$ and $SiO_2$ at a fixed liquid/solid ratio = 50 using a basis of 1000 g $H_2O$. The C-(N-)A-S-H thermodynamic model developed here (CNASH_ss) was used in all simulations. This model is provided as Electronic Supplementary Information, in the correct format for use in GEM-Selektor v3. The data used for the other gases, aqueous species and solid phases included in the simulations, in addition to the C-(N-)A-S-H thermodynamic model developed here, are shown in Appendix C.

## 6.2 Model validation in the $CaO$-$SiO_2$-$H_2O$ system

An extensive body of solubility data for the $CaO$-$SiO_2$-$H_2O$ system is available [2-15], which has been used to develop thermodynamic models for C-S-H gels in the past [15, 17, 18, 22, 25]. The fit of the new model to these data (Figure 2) is very good regarding description of the available data for pH, for concentrations of [Ca] < 2 mmol/L (mM) and [Si] > 0.1 mM, and for Ca and Si solubilities up to a molar Ca/Si ratio in the solid ≈ 1.3. The thermodynamic model is less consistent with the full body of available data at higher dissolved Ca concentrations, lower aqueous Si concentrations, and higher Ca/Si ratios in the solid, but matches more closely with the more recently published data, particularly the measurements reported in [8]. The poorer fit of the thermodynamic model to these data indicate that it is partly limited by the assumption of no additional solid solution $Ca(OH)_2$; the simulated C-S-H gels are in equilibrium with portlandite for Ca/Si > 1.4 and amorphous $SiO_2$ is simulated at Ca/Si ratios in the solid ≤ 0.67 (Figure 2). It has previously been proposed [8] that C-S-H solubility varies as a function of the nanostructure of this phase, which is much more pronounced for Ca/Si > 1 when many nanostructural configurations and potential bonding environments for Ca are

possible (for example, Ca can be accommodated in the *CB* and *IC* sites here). This would mean that C-S-H thermodynamic models with a single curve for the solubility-structure relationships in these gels are inherently unable to describe the full range of available solubility data for this phase. However, the compositional region that is described accurately by the thermodynamic model is the region of principal importance for cementitious materials with compositions in the $CaO$-$Na_2O$-$Al_2O_3$-$SiO_2$-$H_2O$ system, which typically contain C-(N-)A-S-H gels with Ca/Si ≤ 1.2 (as discussed in section 2).

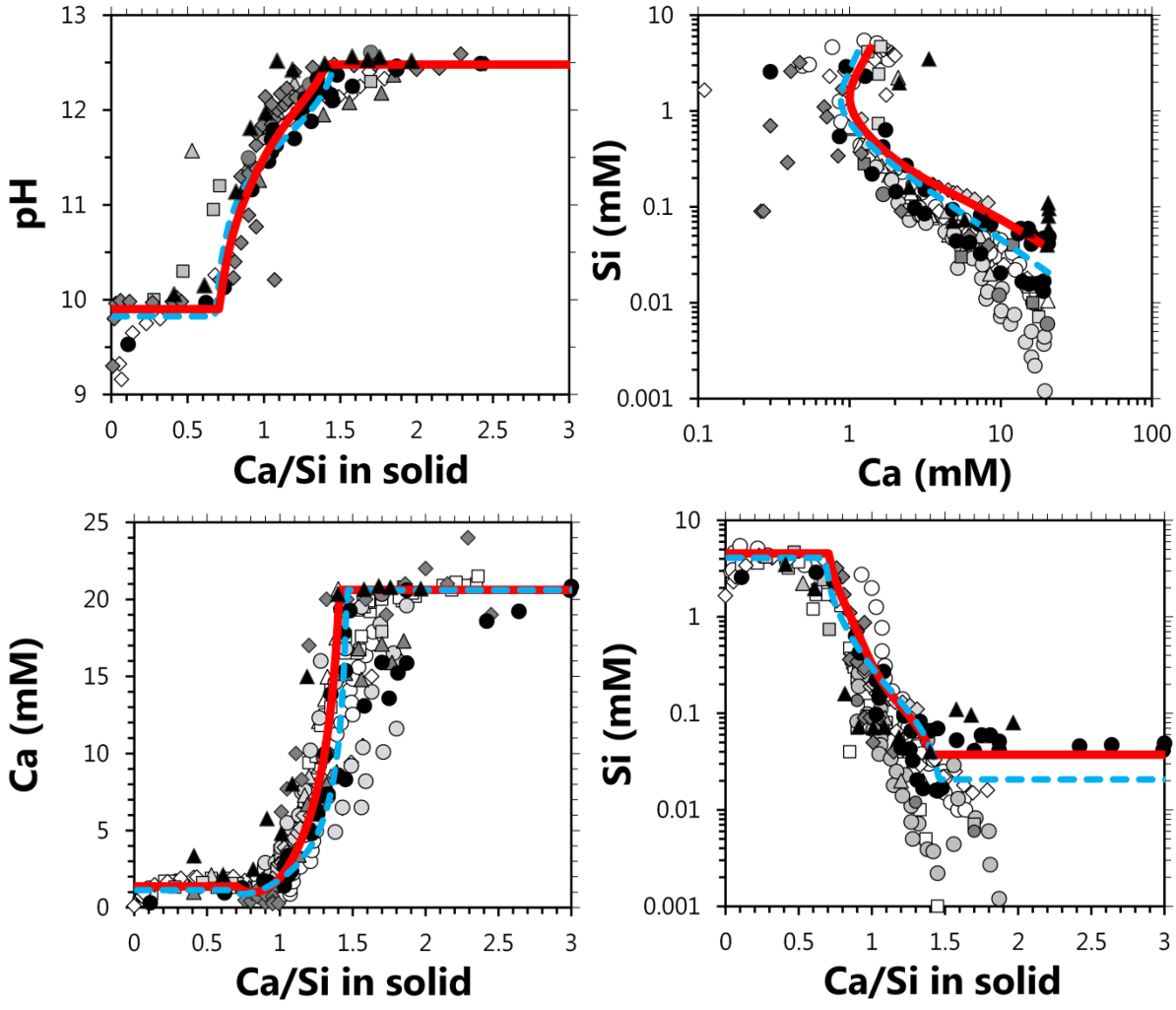

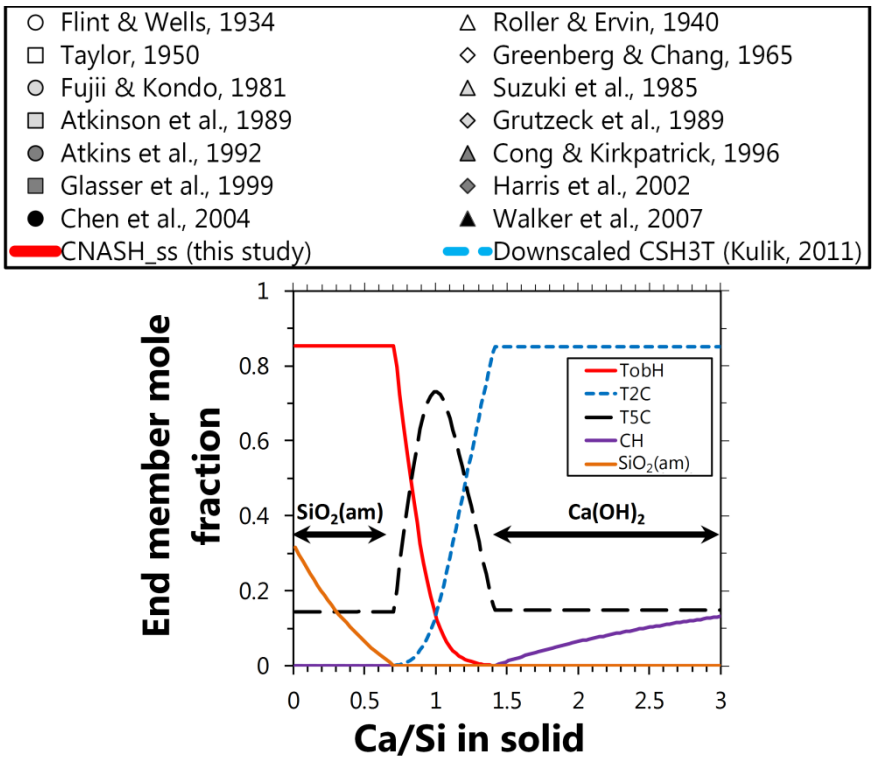


**Figure 2**. Comparison of the simulation results (25°C, 1 bar, water/solids mass ratio = 50) using the thermodynamic model developed here (CNASH_ss, bold red traces) to the downscaled CSH3T model (dashed blue traces) [25] and published solubility data in the CaO-$SiO_2$-$H_2O$ system [2-15]. Additional plots are provided in Appendix D for the MCL and bulk chemistry results. The thermodynamic properties of the phases included in these simulations are given in Appendix C.

## 6.3 Model validation in the CaO-$Na_2O$-$SiO_2$-$H_2O$ system

Significantly fewer thermochemical data are available for cements in the more complex CaO-$Na_2O$-$SiO_2$-$H_2O$ system than in the CaO-$SiO_2$-$H_2O$ system. Simulations for the CaO-$Na_2O$-$SiO_2$-$H_2O$ system (Figure 3) were performed at bulk NaOH concentrations of 0.25, 0.5, 1 and 3 mol/L, and compared to published results in the respective ranges of [NaOH] = 0.1 – 0.3 M, 0.3 – 0.8 M, 0.8 – 1 M, 1 – 5 M. This grouping was chosen to constrain the range of NaOH concentrations in the experimental studies relatively tightly to the bulk alkali concentrations used in the simulations, while maintaining enough data points in each group to enable reliable validation of the thermodynamic model. Results for the 0.5 M NaOH simulation are shown in Figure 3, and the 0.25 M, 1 M and 3 M NaOH simulations are shown in Appendix D.

543 The maximum Ca content of equilibrated (sodium) calcium silicate hydrate (C-(N-)S-H) gels and the
544 bulk system alkalinity are inversely related [75]; C-(N-)S-H gels with solid Ca concentrations above
545 this maximum value are more soluble than portlandite at equilibrium (a maximum value of Ca/Si ≈ 1
546 has been reported for equilibrated C-(N-)S-H gels [75] at bulk NaOH concentrations ≈ 1 mol/kg). The
547 thermodynamic modelling simulations performed here show this same trend (Figure 3 and Appendix
548 D), which indicate that the C-(N-)S-H gels modelled at a bulk NaOH concentration of 3 M are in
549 equilibrium with portlandite at all Ca/Si ratios ≥ 1, rather than the much higher Ca/Si ratios at which
550 this is observed in the $CaO\text{-}SiO_2\text{-}H_2O$ system (Ca/Si ≥ 1.4, Figure 2).
551

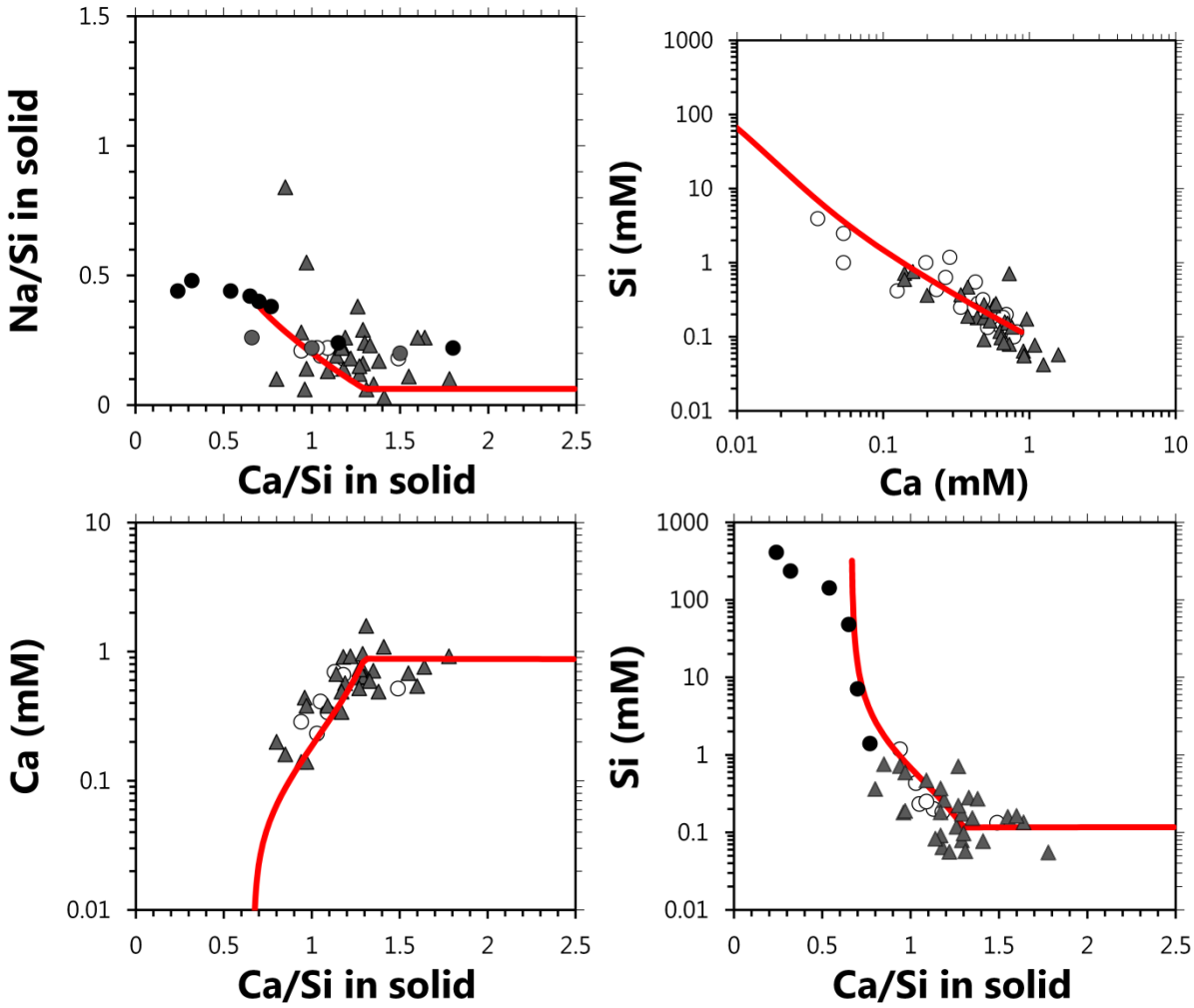

552
553

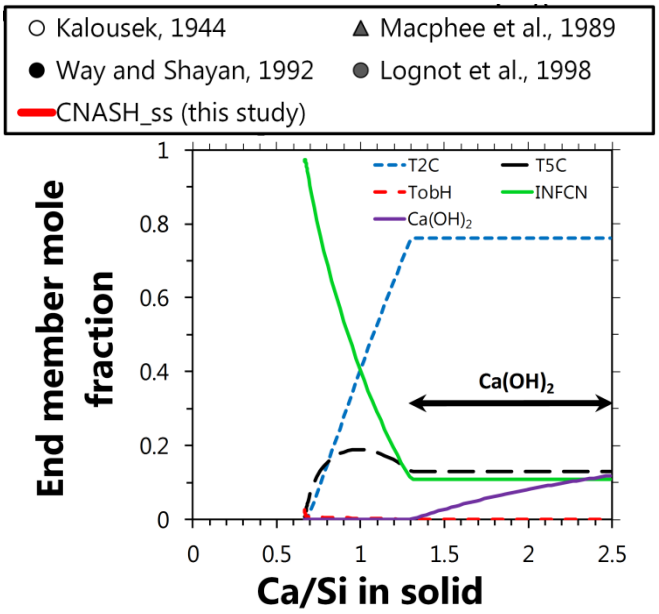


**Figure 3**. Comparison of the simulation results (25°C, 1 bar, 0.5 M NaOH/solids mass ratio = 50) using the thermodynamic model developed here (CNASH_ss, bold red traces) to published solubility data in the $CaO$-$Na_2O$-$SiO_2$-$H_2O$ system at alkali concentrations 0.3 M ≤ [NaOH] ≤ 0.8 M [76, 77, 80, 81]. The simulated C-S-H gels are in equilibrium with portlandite at molar ratios of Ca/Si in the solid ≥ 1.3. Additional plots are provided in Appendix D for the bulk chemistry results. The thermodynamic properties of the phases included in these simulations are given in Appendix C.

The good agreement between the measured solubility data for NaOH concentrations of 0.3 M-0.8 M and the simulation at [NaOH] = 0.5 M is evident in Figure 3. The composition of the simulated C-(N-)S-H gel also captures the relatively higher Na content measured in this phase at lower Ca/Si ratios [77]. The comparisons between the simulated and reported solubility data in the other alkali concentration ranges studied are also good (Appendix D), with the exception of some of the data reported at NaOH concentrations > 1 M in [80]. This may be explained by the presence of additional sodium calcium silicate hydrate gels in those highly alkaline systems that are not described in the thermodynamic databases used here (e.g. phases with similarities to the kanemite group of minerals [85], which are thought to be similar to alkali-aggregate reaction products). This would mean that the aqueous composition data for [NaOH] concentrations > 1 M in [80] may not be solely determined by the solubility of C-(N-)S-H phases.

## 6.4 Model validation in the $CaO-Al_2O_3-SiO_2-H_2O$ system

Analysis of C-A-S-H gel solubility from published solubility data for this phase [41, 86] is complicated by the coexistence of secondary phases such as strätlingite and/or superficial carbonation products (e.g. calcium hemicarboaluminate, $C_4Ac_{0.5}H_{12}$) in the solids analysed. Here, the thermodynamic model is validated against the solubility dataset published by Pardal et al. [41] (Figure 4) over the bulk composition range most relevant for AAS cements, $0.66 \leq Ca/(Al+Si) \leq 1$ and $0 \leq Al/Si \leq 0.33$. The simulation results and the measured solubility data are comparable, to within an order of magnitude. These data show a similar inverse relationship between [Si] and [Ca] to that described by the solubility data for these elements in the $CaO-SiO_2-H_2O$ system (Figure 2).

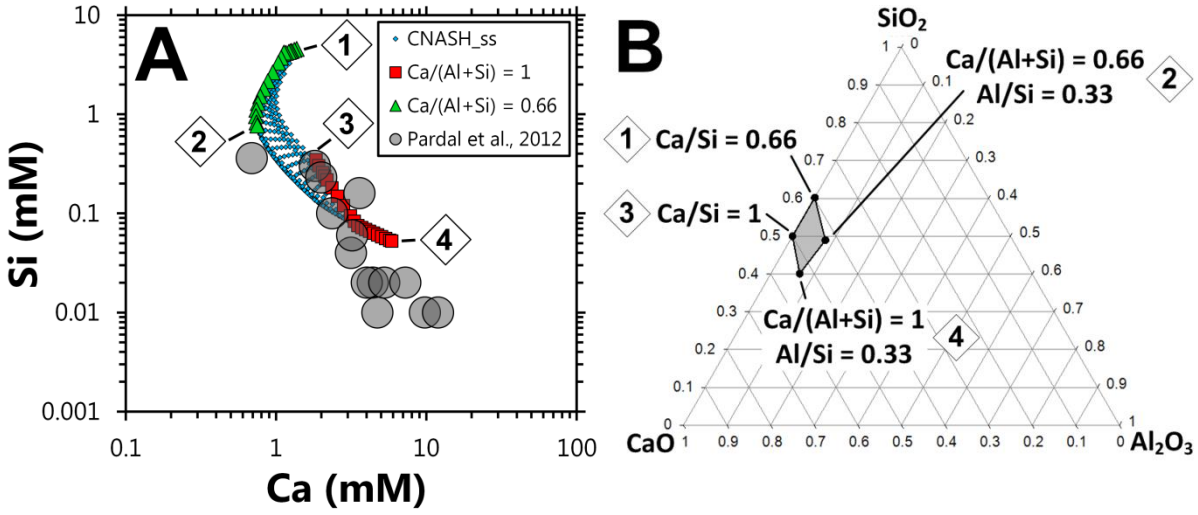


**Figure 4**. A) Comparison of the simulation results (25°C, 1 bar, water/solids mass ratio = 50) using the thermodynamic model developed here (CNASH_ss, small blue diamonds, red squares and green triangles) to published solubility data for C-A-S-H gels in the $CaO-Al_2O_3-SiO_2-H_2O$ system (large grey circles [41]). The corresponding range of bulk compositions simulated, projected onto the $CaO-SiO_2-Al_2O_3$ ternary system, is shown in B). The thermodynamic properties of the phases included in these simulations are given in Appendix C.

Chemical composition data for C-A-S-H gels are also used for model validation [42, 48, 78, 79]; most of these data exist at three bulk Al/Si compositions: Al/Si ≈ 0.1, 0.2 and 0.33. Comparison of the modelling results against these data (Figures 5A-5C), for the relevant composition range in AAS

596 binders (0.65 ≤ bulk Ca/(Al+Si) ≤ 1), shows that the simulations accurately describe all of the
597 reported chemical composition data for this phase.
598

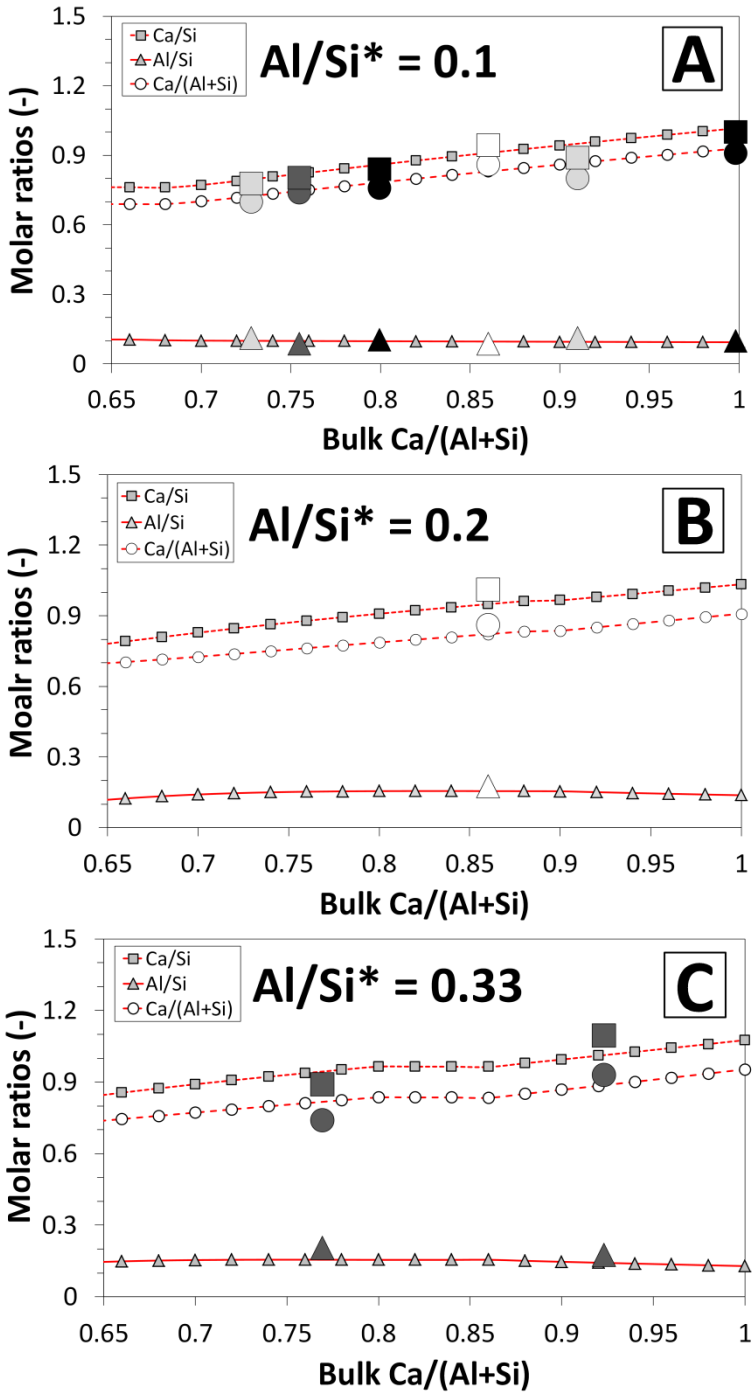


599
600
601

602 **Figure 5**. Comparison of the simulation results (25°C, 1 bar, water/solids mass ratio = 50) using the
603 thermodynamic model developed here (CNASH_ss, small symbols and red lines) to the published
604 chemical composition data for C-A-S-H gels (large symbols represent data from the literature: white
605 [42]; light grey [78]; dark grey [48]; black [79]). Al/Si* = bulk Al/Si. Additional plots are provided in

606 Appendix D for the end-member compositions. The thermodynamic properties of the phases
607 included in these simulations are given in Appendix C.
608

609 ## 6.5 Model validation in AAS cement systems

610 Simulations for calculating the solubility of AAS cements were performed in an $N_2$ atmosphere (1 g of
611 $N_{2\ (g)}$, to avoid oxidation of the system) at 25°C, 1 bar and at water/binder ratios specified as
612 reported in the literature (Appendix E). Congruent slag dissolution was assumed, with the slag
613 reaction extents and bulk chemical compositions simulated by proportional additions of $SiO_2$, CaO,
614 MgO, $Al_2O_3$, $Na_2O$, $K_2O$, and $H_2SO_4$ or dissociated $H_2S_{(aq)}$ (matching the $SO_4^{2-}$ and $S^{2-}$ content in the
615 slag where reported, otherwise all sulfur is assumed to be present as $S^{2-}$), to match the bulk slag
616 chemical compositions and reaction extents reported in the literature (e.g. [45, 87, 88]). All other
617 components of the slag were excluded, as the concentrations of other elements in the slags studied
618 are minor and the reactivity of Fe entrained in slag appears to be very low [89]. For the cases where
619 the degree of reaction of the slag is needed but not available, the extent of reaction of the slag was
620 set so that the bulk chemistry of the simulations matched the bulk chemistry of the binder gel
621 assumed in the original work [50], or estimated where no further information was available (using
622 the reaction extents provided in [87] as reference values, then modifying based on the bulk alkalinity
623 and curing time).
624

625 The simulated solubility results (Figure 6) match the experimentally-measured solubility data to
626 approximately ±1 order of magnitude, with the poorest agreement found for the aqueous Si species
627 in $Na_2O{\cdot}mSiO_2{\cdot}xH_2O$-activated cements, which are under-predicted by the thermodynamic model.
628 However, the uncertainty associated with each experimental data point is expected to be large,
629 possibly also up to one order of magnitude, because slag reaction extents are not quantified in the
630 experimental studies referenced here (with the exception of the estimations in [87] for the data in
631 [71]) and the data correspond to systems that are quite far from equilibrium in some cases (e.g.
632 samples were cured for 7 days in [82]). Similar slag reaction degrees to those estimated here (~40%

at 100 days of curing) have been observed in sodium silicate and NaOH-activated slag pastes (35%-45% at 100 days of curing [44]), which does indicate that the estimates used here are reasonable, but does not fully resolve the uncertainty attributed to this factor. With this in mind, the accuracy of the fit between the simulation and experimental results is similar to the level of uncertainty that can be expected for modelling dissolved elemental concentrations in AAS cements.

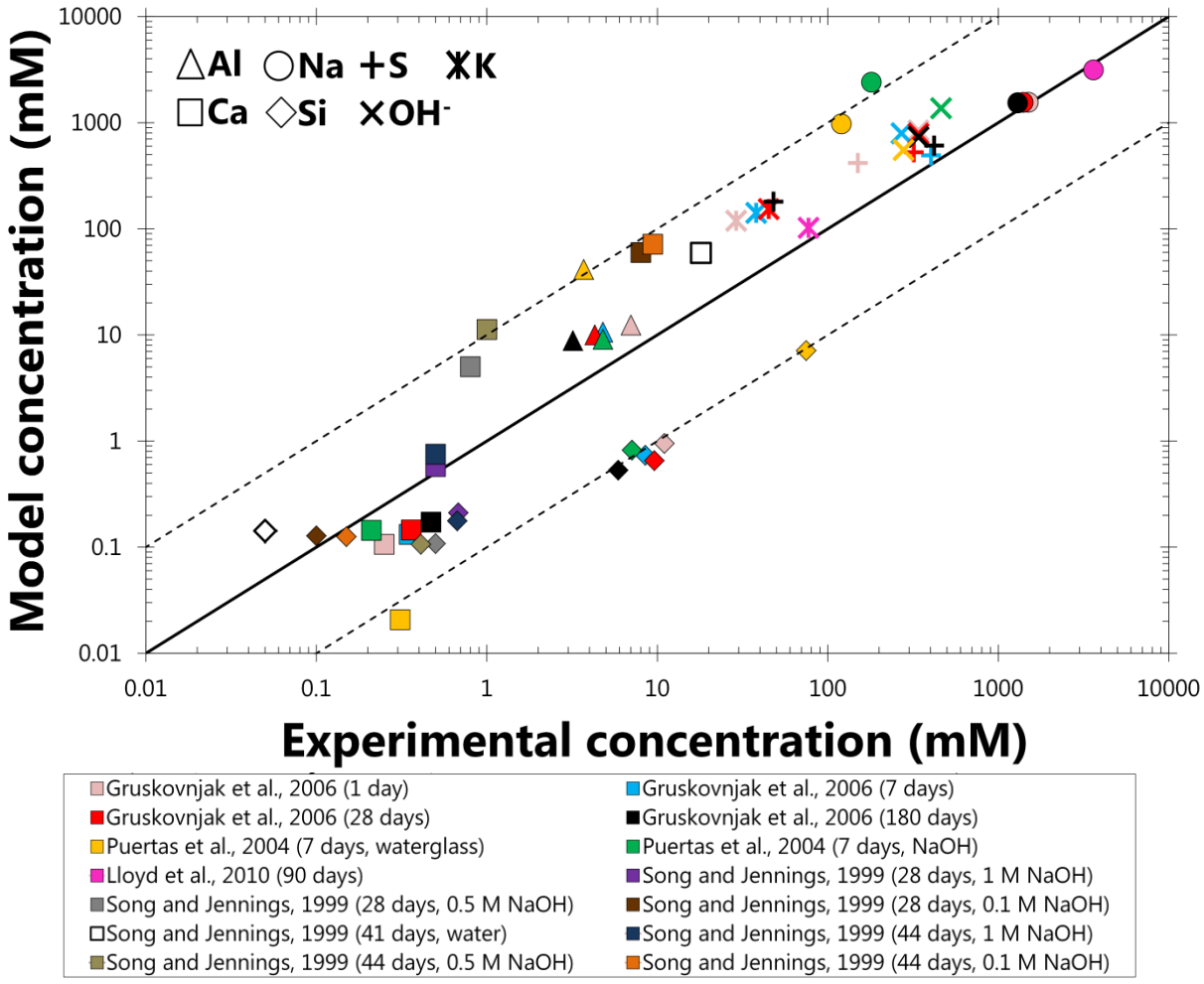


**Figure 6**. Simulated elemental concentrations in the aqueous phase compared to experimental pore solution composition data for AAS cements [71, 82-84]. The dotted lines show ±1 order of magnitude deviation from the solid y = x line. The thermodynamic properties of the phases included in these simulations are given in Appendix C. The slag reaction extents used in these simulations are shown in Appendix E.

Comparisons between thermodynamic modelling results and experimental measurements of C-(N-)A-S-H gel chemical compositions in AAS cements are not straightforward because secondary

649 products are often intimately intermixed with C-(N-)A-S-H gel in these materials [27] and because
650 the nanostructure and chemical composition of this phase can vary considerably at extended ages
651 [39]. In this sense, thermodynamic modelling can play an important role in understanding how the
652 solid phase assemblage and chemical composition of C-(N-)A-S-H gel may change over time, with
653 simulation results representing the predicted nature of the solid binder at equilibrium.
654
655 It is also important to assess how accurately the thermodynamic model represents the bulk
656 volumetric properties of C-(N-)A-S-H gels, because this is a central aspect of the application of
657 thermodynamic modelling to cement-based materials [90]. The C-(N-)A-S-H gels formed in AAS
658 cements are significantly denser than the C-S-H gels formed in neat PC materials [50], which is a
659 result that should be embodied in thermodynamic models for this phase. Hence simulations using
660 the thermodynamic model developed here are compared to the available volumetric data for C-(N-
661 )A-S-H gels in AAS cements (Table 3).
662
663 **Table 3**. Simulated C-(N-)A-S-H gel properties in AAS cements [45, 50, 88] compared to the results
664 reported in [50], using the bulk chemistry described in that study. The thermodynamic properties of
665 the relevant phases in these simulations are given in Appendix C.

| Activator | Curing time (days) | Density (g/cm$^3$) | Molar volume (cm$^3$/mol Si in C-(N-)A-S-H) | Reference |
|---|---|---|---|---|
| | | **Experimental values** | | |
| $Na_2O{\cdot}1.82SiO_2{\cdot}xH_2O$ | 90 | 2.73 | 50.8 | [50] |
| | | **Simulated values** | | |
| $Na_2O{\cdot}1.82SiO_2{\cdot}xH_2O$ | 90 | 2.6 | 58 | [50] |
| $Na_2SiO_3$ | 180 | 2.7 | 53 | COL-GBFS, [88] |
| $Na_2SiO_3$ | 180 | 2.7 | 54 | AUS-GBFS, [88] |
| $Na_2SiO_3$ | 180 | 2.7 | 53 | SP-GBFS, [88] |
| NaOH | 100 | 2.6 | 57 | [45] |
| $Na_2SiO_3{\cdot}5H_2O$ | 100 | 2.5 | 56 | [45] |

666
667 The C-(N-)A-S-H bulk densities and molar volumes simulated by thermodynamic modelling are
668 similar to the reported volumetric properties of this phase (Table 3) [50]. This result is consistent
669 with a much more tightly packed atomic structure for the C-(N-)A-S-H gels formed in AAS cements
670 than for the C-S-H gels formed in neat PC materials ($(CaO)_{1.7}(SiO_2)_1(H_2O)_{1.8}$, molar volume = 72.1

671 $cm^3$/mol [91]). This is also consistent with the discussion presented in [50], where it was argued that
672 the reported density and molar volume of the C-S-H type gels formed in AAS cements are only
673 weakly related to the bulk composition of these materials. Therefore, it can be expected that the
674 thermodynamic model developed here is able to closely represent the bulk volumetric properties of
675 C-(N-)A-S-H gels in AAS cements.
676

677 ## 6.6 Discussion and perspectives

678 This paper represents the first step towards developing a structurally-consistent thermodynamic
679 model for C-(N-)A-S-H gel that contains explicit descriptions of Al and alkali components, which
680 provides a relatively simple basis for further development and utilisation. Therefore, there are a
681 number of aspects that would improve the thermodynamic model, and some are listed here to guide
682 future development:

683 - The thermodynamic model has been designed for C-(N-)A-S-H gels with significant Al and
684 alkali incorporation, particularly those formed in AAS cement. This model may also be
685 relevant to high volume blended PC/SCM materials reacted with either water or an alkali
686 source (e.g. CEM III blast furnace cements as specified in EN 197-1), as the bulk chemical
687 compositions of these materials and AAS cements can be similar (Ca/(Al+Si) ≈ 1) [92]. Its
688 suitability for use in simulating the chemistry of these materials needs to be assessed
689 further.
690 - Improvement can be found by removing the assumptions used to simplify the mixing
691 relationships for the sublattice solid solution model, which approximated the Gibbs free
692 energies of the reciprocal reactions and the excess Gibbs free energies to zero. This will
693 become possible as more information is obtained about the energetic differences arising
694 between hypothetical end-members (i.e. energetic information regarding Si-for-Al
695 substitution in chain sites, and ($Ca^{2+}$,$2Na^{+}$,$2H^{+}$) substitution in interlayer sites) and the
696 solubility of C-(N-)A-S-H gels.

- The utility of the pore solution composition data used to parameterise the thermodynamic model in AAS cements would be significantly improved if such data were published alongside quantification of the reaction extent of the slag. This information, along with more solubility data for AAS cements and synthetic CaO-$Na_2O$-$Al_2O_3$-$SiO_2$-$H_2O$ systems, will be needed to enable further development of thermodynamic models for C-(N-)A-S-H gels.

# 7. Conclusions

This paper has presented a thermodynamic model for the C-(N-)A-S-H gel in AAS cements, which for the first time accounts explicitly for the structurally-incorporated Al and Na species in this phase. This model represents C-(N-)A-S-H gel as an ideal solid solution of tobermorite-like end-members with independent substitution of tetrahedral Al and Na species allowed in its formulation, meaning that it may also be applicable to cement-based materials that are less alkali- and/or Al-rich than AAS cements. The model was implemented in GEM-Selektor using thermodynamic properties for the C-(N-)A-S-H end-members that were parameterised to match a comprehensive set of solubility data in the CaO-($Na_2O$,$Al_2O_3$)-$SiO_2$-$H_2O$ and AAS cement systems, and published chemical compositions of C-A-S-H gels.

A good fit was found between the full set of data used in the parameterisation procedure and the simulation results, which were within ±1 order of magnitude in simulations of aqueous phase chemical compositions in AAS cements, indicating that the model is suitable for thermodynamic modelling of these materials. The molar volume and density of the C-(N-)A-S-H gels simulated by the model were also in close agreement with the available data for this phase in AAS cements, meaning that the model can describe chemical shrinkage in these systems. Therefore, the thermodynamic model developed here greatly improves the scope of thermodynamic modelling applications to Ca-

rich alkali-activated cements and hybrid alkali-activated/PC materials, which is important for understanding the durability of these materials under sealed, ambient and aggressive environmental conditions.

## 8. Supporting information

The GEM-Selektor database files for the thermodynamic model developed here (CNASH_ss) are provided as Electronic Supplementary Information, which can be accessed via the journal website (http://www.journals.elsevier.com/cement-and-concrete-research/).

## 9. Acknowledgements

Special thanks are due to D. A. Kulik, as his contributions on thermodynamic modelling of C-S-H gels provided the basis for this work [17, 25], to the team behind the freely available GEM-Selektor thermodynamic modelling program (http://gems.web.psi.ch/) [61, 62], and to those involved in the development of the thermodynamic database for cement related phases (CEMDATA) [17, 23, 64-69]. The authors would also like to thank the anonymous reviewers of this paper, whose comments helped to substantially improve its quality and rigour.

## 10. References

[1] H.F.W. Taylor, Cement Chemistry, 2nd ed., Thomas Telford Publishing, London, 1997.

[2] E.P. Flint, L.S. Wells, Study of the system $CaO-SiO_2-H_2O$ at 30°C and of the reaction of water on the anhydrous calcium silicates, J. Res. Natl. Bur. Stand., 12 (1934) 751-783.

[3] H.F.W. Taylor, Hydrated calcium silicates. Part I. Compound formation at ordinary temperatures, J. Chem. Soc., (1950) 3682-3690.

[4] K. Fujii, W. Kondo, Heterogeneous equilibrium of calcium silicate hydrate in water at 30°C, J. Chem. Soc., Dalton Trans., (1981) 645-651.

[5] A. Atkinson, J.A. Hearne, C.F. Knights, Aqueous chemistry and thermodynamic modelling of $CaO-SiO_2-H_2O$ gels, J. Chem. Soc., Dalton Trans., (1989) 2371-2379.

[6] M. Atkins, F.P. Glasser, A. Kindness, Cement hydrate phase: solubility at 25°C, Cem. Concr. Res., 22 (1992) 241-246.

[7] F.P. Glasser, M. Tyrer, K. Quillin, D. Ross, J. Pedersen, K. Goldthorpe, D. Bennett, M. Atkins, The chemistry of blended cements and backfills intended for use in radioactive waste disposal: R&D technical report P98, Bristol, 1999.

[8] J.J. Chen, J.J. Thomas, H.F.W. Taylor, H.M. Jennings, Solubility and structure of calcium silicate hydrate, Cem. Concr. Res., 34 (2004) 1499-1519.

[9] P.S. Roller, G. Ervin, The system calcium oxide-silica-water at 30°C. The association of silicate ion in dilute alkaline solution, J. Am. Chem. Soc., 62 (1940) 461-471.

[10] S.A. Greenberg, T.N. Chang, Investigation of the colloidal hydrated calcium silicates. II. Solubility relationships in the calcium oxide-silica-water system at 25°C, J. Phys. Chem., 69 (1965) 182-188.

[11] K. Suzuki, T. Nishikawa, S. Ito, Formation and carbonation of C-S-H in water, Cem. Concr. Res., 15 (1985) 213-224.

[12] M. Grutzeck, A. Benesi, B. Fanning, Silicon-29 magic angle spinning nuclear magnetic resonance study of calcium silicate hydrates, J. Am. Ceram. Soc., 72 (1989) 665-668.

[13] X. Cong, R.J. Kirkpatrick, $^{29}Si$ MAS NMR study of the structure of calcium silicate hydrate, Adv. Cem. Based Mater., 3 (1996) 144-156.

[14] A.W. Harris, M.C. Manning, W.M. Tearle, C.J. Tweed, Testing of models of the dissolution of cements—leaching of synthetic CSH gels, Cem. Concr. Res., 32 (2002) 731-746.

[15] C.S. Walker, D. Savage, M. Tyrer, K.V. Ragnarsdottir, Non-ideal solid solution aqueous solution modeling of synthetic calcium silicate hydrate, Cem. Concr. Res., 37 (2007) 502-511.

[16] H.M. Jennings, Aqueous solubility relationships for two types of calcium silicate hydrate, J. Am. Ceram. Soc., 69 (1986) 614-618.

[17] D.A. Kulik, M. Kersten, Aqueous solubility diagrams for cementitious waste stabilization systems: II. End-member stoichiometries of ideal calcium silicate hydrate solid solutions, J. Am. Ceram. Soc., 84 (2001) 3017-3026.

[18] U.R. Berner, Evolution of pore water chemistry during degradation of cement in a radioactive waste repository environment, Waste Manage., 12 (1992) 201-219.

785 [19] F.P. Glasser, E.E. Lachowski, D.E. Macphee, Compositional model for calcium silicate hydrate
786 (C-S-H) gels, their solubilities, and free energies of formation, J. Am. Ceram. Soc., 70 (1987)
787 481-485.

788 [20] E.J. Reardon, An ion interaction model for the determination of chemical equilibria in
789 cement/water systems, Cem. Concr. Res., 20 (1990) 175-192.

790 [21] M. Atkins, D.G. Bennett, A.C. Dawes, F.P. Glasser, A. Kindness, D. Read, A thermodynamic
791 model for blended cements, Cem. Concr. Res., 22 (1992) 497-502.

792 [22] J.A. Gisby, R.H. Davies, A.T. Dinsdale, M. Tyrer, F.P. Glasser, J. Hill, P. Livesey, C. Walker, C-S-
793 H solubility modeling at different temperatures, in: Proceedings of the 12th International
794 Congress on the Chemistry of Cement, Cement Association of Canada, Montreal, 2007.

795 [23] B. Lothenbach, F. Winnefeld, Thermodynamic modelling of the hydration of Portland
796 cement, Cem. Concr. Res., 36 (2006) 209-226.

797 [24] B. Lothenbach, Thermodynamic equilibrium calculations in cementitious systems, Mater.
798 Struct., 43 (2010) 1413-1433.

799 [25] D.A. Kulik, Improving the structural consistency of C-S-H solid solution thermodynamic
800 models, Cem. Concr. Res., 41 (2011) 477-495.

801 [26] B. Lothenbach, K. Scrivener, R.D. Hooton, Supplementary cementitious materials, Cem.
802 Concr. Res., 41 (2011) 1244-1256.

803 [27] I.G. Richardson, G.W. Groves, Microstructure and microanalysis of hardened cement pastes
804 involving ground granulated blast-furnace slag, J. Mater. Sci., 27 (1992) 6204-6212.

805 [28] J.L. Provis, S.A. Bernal, Geopolymers and related alkali-activated materials, Annu. Rev.
806 Mater. Res., 44 (2014) 3.1-3.29.

807 [29] C. Shi, P.V. Krivenko, D. Roy, Alkali-Activated Cements and Concretes, 1st ed., Taylor &
808 Francis, New York, 2006.

809 [30] M. Atkins, F. Glasser, L.P. Moroni, J.J. Jack, Thermodynamic modelling of blended cements at
810 elevated temperature (50-90°C), Aberdeen University, United Kingdom,
811 DoE1HMIP1RR/94.011, 1994.

812 [31] M. Ben Haha, B. Lothenbach, G. Le Saoût, F. Winnefeld, Influence of slag chemistry on the
813 hydration of alkali-activated blast-furnace slag - part II: effect of $Al_2O_3$, Cem. Concr. Res., 42
814 (2012) 74-83.

815 [32] W. Loewenstein, The distribution of aluminum in the tetrahedra of silicates and aluminates,
816 Am. Mineral., 39 (1954) 92-96.

817 [33] L. Pegado, C. Labbez, S.V. Churakov, Mechanism of aluminium incorporation into C-S-H from
818 ab initio calculations, J. Mater. Chem. A, 2 (2014) 3477-3483.

819 [34] I.G. Richardson, A.R. Brough, R. Brydson, G.W. Groves, C.M. Dobson, Location of aluminum
820 in substituted calcium silicate hydrate (C-S-H) gels as determined by $^{29}Si$ and $^{27}Al$ NMR and
821 EELS, J. Am. Ceram. Soc., 76 (1993) 2285-2288.

[35] I.G. Richardson, A.R. Brough, G.W. Groves, C.M. Dobson, The characterization of hardened alkali-activated blast-furnace slag pastes and the nature of the calcium silicate hydrate (C-S-H) phase, Cem. Concr. Res., 24 (1994) 813-829.

[36] F. Puertas, M. Palacios, H. Manzano, J.S. Dolado, A. Rico, J. Rodríguez, A model for the C-A-S-H gel formed in alkali-activated slag cements, J. Eur. Ceram. Soc., 31 (2011) 2043-2056.

[37] F. Bonk, J. Schneider, M.A. Cincotto, H. Panepucci, Characterization by multinuclear high-resolution NMR of hydration products in activated blast-furnace slag pastes, J. Am. Ceram. Soc., 86 (2003) 1712-1719.

[38] I.G. Richardson, G.W. Groves, The incorporation of minor and trace elements into calcium silicate hydrate (C-S-H) gel in hardened cement pastes, Cem. Concr. Res., 23 (1993) 131-138.

[39] R.J. Myers, S.A. Bernal, R. San Nicolas, J.L. Provis, Generalized structural description of calcium-sodium aluminosilicate hydrate gels: the cross-linked substituted tobermorite model, Langmuir, 29 (2013) 5294-5306.

[40] A. Fernández-Jiménez, F. Puertas, I. Sobrados, J. Sanz, Structure of calcium silicate hydrates formed in alkaline-activated slag: Influence of the type of alkaline activator, J. Am. Ceram. Soc., 86 (2003) 1389-1394.

[41] X. Pardal, F. Brunet, T. Charpentier, I. Pochard, A. Nonat, $^{27}$Al and $^{29}$Si solid-state NMR characterization of calcium-aluminosilicate-hydrate, Inorg. Chem., 51 (2012) 1827-1836.

[42] G.K. Sun, J.F. Young, R.J. Kirkpatrick, The role of Al in C-S-H: NMR, XRD, and compositional results for precipitated samples, Cem. Concr. Res., 36 (2006) 18-29.

[43] S.D. Wang, K.L. Scrivener, Hydration products of alkali activated slag cement, Cem. Concr. Res., 25 (1995) 561-571.

[44] M. Ben Haha, G. Le Saoût, F. Winnefeld, B. Lothenbach, Influence of activator type on hydration kinetics, hydrate assemblage and microstructural development of alkali activated blast-furnace slags, Cem. Concr. Res., 41 (2011) 301-310.

[45] G. Le Saoût, M. Ben Haha, F. Winnefeld, B. Lothenbach, Hydration degree of alkali-activated slags: a $^{29}$Si NMR study, J. Am. Ceram. Soc., 94 (2011) 4541-4547.

[46] A.R. Brough, A. Atkinson, Sodium silicate-based, alkali-activated slag mortars - Part I. Strength, hydration and microstructure, Cem. Concr. Res., 32 (2002) 865-879.

[47] X. Pardal, I. Pochard, A. Nonat, Experimental study of Si-Al substitution in calcium-silicate-hydrate (C-S-H) prepared under equilibrium conditions, Cem. Concr. Res., 39 (2009) 637-643.

[48] P. Faucon, A. Delagrave, J.C. Petit, C. Richet, J.M. Marchand, H. Zanni, Aluminum incorporation in calcium silicate hydrates (C-S-H) depending on their Ca/Si ratio, J. Phys. Chem. B, 103 (1999) 7796-7802.

[49] H.M. Jennings, Refinements to colloid model of C-S-H in cement: CM-II, Cem. Concr. Res., 38 (2008) 275-289.

858 [50] J.J. Thomas, A.J. Allen, H.M. Jennings, Density and water content of nanoscale solid C-S-H
859 formed in alkali-activated slag (AAS) paste and implications for chemical shrinkage, Cem.
860 Concr. Res., 42 (2012) 377-383.

861 [51] E. Bonaccorsi, S. Merlino, A.R. Kampf, The crystal structure of tobermorite 14Å (plombierite),
862 a C-S-H phase, J. Am. Ceram. Soc., 88 (2005) 505-512.

863 [52] S. Merlino, E. Bonaccorsi, T. Armbruster, The real structure of tobermorite 11Å: normal and
864 anomalous forms, OD character and polytypic modifications, Eur. J. Mineral., 13 (2001) 577-
865 590.

866 [53] I.G. Richardson, Tobermorite/jennite- and tobermorite/calcium hydroxide-based models for
867 the structure of C-S-H: applicability to hardened pastes of tricalcium silicate, β-dicalcium
868 silicate, Portland cement, and blends of Portland cement with blast-furnace slag,
869 metakaolin, or silica fume, Cem. Concr. Res., 34 (2004) 1733-1777.

870 [54] I.G. Richardson, The calcium silicate hydrates, Cem. Concr. Res., 38 (2008) 137-158.

871 [55] I.G. Richardson, G.W. Groves, Models for the composition and structure of calcium silicate
872 hydrate (CSH) gel in hardened tricalcium silicate pastes, Cem. Concr. Res., 22 (1992) 1001-
873 1010.

874 [56] A.J. Allen, J.J. Thomas, H.M. Jennings, Composition and density of nanoscale calcium-silicate-
875 hydrate in cement, Nat. Mater., 6 (2007) 311-316.

876 [57] M. Hillert, Phase equilibria, phase diagrams and phase transformations: their
877 thermodynamic basis, Cambridge University Press, Cambridge, 1998.

878 [58] M. Hillert, L.-I. Staffansson, The regular solution model for stoichiometric phases and ionic
879 melts, Acta Chem. Scand., 24 (1970) 3618-3626.

880 [59] J.O. Andersson, A.F. Guillermet, M. Hillert, B. Jansson, B. Sundman, A compound-energy
881 model of ordering in a phase with sites of different coordination numbers, Acta Metall.
882 Mater., 34 (1986) 437-445.

883 [60] J.L. Provis, P. Duxson, G.C. Lukey, J.S.J. Van Deventer, Statistical thermodynamic model for
884 Si/Al ordering in amorphous aluminosilicates, Chem. Mater., 17 (2005) 2976-2986.

885 [61] D.A. Kulik, T. Wagner, S.V. Dmytrieva, G. Kosakowski, F.F. Hingerl, K.V. Chudnenko, U.
886 Berner, GEM-Selektor geochemical modeling package: revised algorithm and GEMS3K
887 numerical kernel for coupled simulation codes, Comput. Geosci., 17 (2013) 1-24.

888 [62] T. Wagner, D.A. Kulik, F.F. Hingerl, S.V. Dmytrieva, GEM-Selektor geochemical modeling
889 package: TSolMod library and data interface for multicomponent phase models, Can.
890 Mineral., 50 (2012) 1173-1195.

891 [63] W. Hummel, U. Berner, E. Curti, F.J. Pearson, T. Thoenen, Nagra/PSI Chemical
892 Thermodynamic Database 01/01, Universal Publishers, Parkland, 2002.

893 [64] T. Matschei, B. Lothenbach, F.P. Glasser, Thermodynamic properties of Portland cement
894 hydrates in the system $CaO-Al_2O_3-SiO_2-CaSO_4-CaCO_3-H_2O$, Cem. Concr. Res., 37 (2007) 1379-
895 1410.

[65] T. Schmidt, B. Lothenbach, M. Romer, K. Scrivener, D. Rentsch, R. Figi, A thermodynamic and experimental study of the conditions of thaumasite formation, Cem. Conc. Res., 38 (2008) 337-349.

[66] B. Lothenbach, T. Matschei, G. Möschner, F.P. Glasser, Thermodynamic modelling of the effect of temperature on the hydration and porosity of Portland cement, Cem. Concr. Res., 38 (2008) 1-18.

[67] D.A. Kulik, M. Kersten, Aqueous solubility diagrams for cementitious waste stabilization systems. 4. A carbonation model for Zn-doped calcium silicate hydrate by Gibbs energy minimization, Environ. Sci. Technol., 36 (2002) 2926-2931.

[68] G. Möschner, B. Lothenbach, J. Rose, A. Ulrich, R. Figi, R. Kretzschmar, Solubility of Fe–ettringite ($Ca_6[Fe(OH)_6]_2(SO_4)_3 \cdot 26H_2O$), Geochim. Cosmochim. Acta, 72 (2008) 1-18.

[69] G. Möschner, B. Lothenbach, F. Winnefeld, A. Ulrich, R. Figi, R. Kretzschmar, Solid solution between Al-ettringite and Fe-ettringite ($Ca_6[Al_{1-x}Fe_x(OH)_6]_2(SO_4)_3 \cdot 26H_2O$), Cem. Concr. Res., 39 (2009) 482-489.

[70] H.C. Helgeson, D.H. Kirkham, G.C. Flowers, Theoretical prediction of the thermodynamic behavior of aqueous electrolytes at high pressures and temperatures: IV. Calculation of activity coefficients, osmotic coefficients, and apparent molal and standard and relative partial molal properties to 600°C and 5 kb, Am. J. Sci., 281 (1981) 1249-1516.

[71] A. Gruskovnjak, B. Lothenbach, L. Holzer, R. Figi, F. Winnefeld, Hydration of alkali-activated slag: Comparison with ordinary Portland cement, Adv. Cem. Res., 18 (2006) 119-128.

[72] K.S. Pitzer, Ion interaction approach: theory and data correlation, in: Activity Coefficients in Electrolyte Solutions, CRC Press, Boca Raton, 1991, 75-153.

[73] J.L. Provis, P. Duxson, G.C. Lukey, F. Separovic, W.M. Kriven, J.S.J. Van Deventer, Modeling speciation in highly concentrated alkaline silicate solutions, Ind. Eng. Chem. Res., 44 (2005) 8899-8908.

[74] G.M. Anderson, D.A. Crerar, Thermodynamics in geochemistry: the equilibrium model, Oxford University Press, Oxford, 1993.

[75] I. Lognot, I. Klur, A. Nonat, NMR and infrared spectroscopies of C-S-H and Al-substituted C-S-H synthesised in alkaline solutions, in: P. Colombet, H. Zanni, A.-R. Grimmer, P. Sozzani (Eds.) Nuclear magnetic resonance spectroscopy of cement-based materials, Springer Berlin Heidelberg, 1998, 189-196.

[76] S.Y. Hong, F.P. Glasser, Alkali binding in cement pastes: part I. The C-S-H phase, Cem. Concr. Res., 29 (1999) 1893-1903.

[77] S.J. Way, A. Shayan, Study of some synthetically prepared hydrous alkali calcium silicates, Cem. Concr. Res., 22 (1992) 915-926.

[78] G. Renaudin, J. Russias, F. Leroux, F. Frizon, C. Cau-dit-Coumes, Structural characterization of C-S-H and C-A-S-H samples - part I: long-range order investigated by Rietveld analyses, J. Solid State Chem., 182 (2009) 3312-3319.

[79] G. Renaudin, J. Russias, F. Leroux, C. Cau-dit-Coumes, F. Frizon, Structural characterization of C-S-H and C-A-S-H samples - part II: local environment investigated by spectroscopic analyses, J. Solid State Chem., 182 (2009) 3320-3329.

[80] G.L. Kalousek, Studies of portions of the quaternary system soda-lime-silica-water at 25°C, J. Res. Natl. Bur. Stand., 32 (1944) 285-302.

[81] D.E. Macphee, K. Luke, F.P. Glasser, E.E. Lachowski, Solubility and aging of calcium silicate hydrates in alkaline solutions at 25°C, J. Am. Ceram. Soc., 72 (1989) 646-654.

[82] F. Puertas, A. Fernández-Jiménez, M.T. Blanco-Varela, Pore solution in alkali-activated slag cement pastes. Relation to the composition and structure of calcium silicate hydrate, Cem. Concr. Res., 34 (2004) 139-148.

[83] R.R. Lloyd, J.L. Provis, J.S.J. van Deventer, Pore solution composition and alkali diffusion in inorganic polymer cement, Cem. Concr. Res., 40 (2010) 1386-1392.

[84] S. Song, H.M. Jennings, Pore solution chemistry of alkali-activated ground granulated blast-furnace slag, Cem. Concr. Res., 29 (1999) 159-170.

[85] R.J. Kirkpatrick, A.G. Kalinichev, X. Hou, L. Struble, Experimental and molecular dynamics modeling studies of interlayer swelling: water incorporation in kanemite and ASR gel, Mater. Struct., 38 (2005) 449-458.

[86] P. Faucon, J.C. Petit, T. Charpentier, J.F. Jacquinot, F. Adenot, Silicon Substitution for Aluminum in Calcium Silicate Hydrates, J. Am. Ceram. Soc., 82 (1999) 1307-1312.

[87] B. Lothenbach, A. Gruskovnjak, Hydration of alkali-activated slag: thermodynamic modelling, Adv. Cem. Res., 19 (2007) 81-92.

[88] S.A. Bernal, R. San Nicolas, R.J. Myers, R. Mejía de Gutiérrez, F. Puertas, J.S.J. van Deventer, J.L. Provis, MgO content of slag controls phase evolution and structural changes induced by accelerated carbonation in alkali-activated binders, Cem. Concr. Res., 57 (2014) 33-43.

[89] S.A. Bernal, V. Rose, J.L. Provis, The fate of iron in blast furnace slag particles during alkali-activation, Mater. Chem. Phys., 146 (2014) 1-5.

[90] B. Lothenbach, G. Le Saout, E. Gallucci, K. Scrivener, Influence of limestone on the hydration of Portland cements, Cem. Concr. Res., 38 (2008) 848-860.

[91] A.J. Allen, J.J. Thomas, Analysis of C-S-H gel and cement paste by small-angle neutron scattering, Cem. Concr. Res., 37 (2007) 319-324.

[92] R. Taylor, I.G. Richardson, R.M.D. Brydson, Composition and microstructure of 20-year-old ordinary Portland cement-ground granulated blast-furnace slag blends containing 0 to 100% slag, Cem. Concr. Res., 40 (2010) 971-983.

[93] R.A. Robie, B.S. Hemingway, Thermodynamic properties of minerals and related substances at 298.15 K and 1 bar ($10^5$ Pascals) pressure and at higher temperatures, United States Government Printing Office, Washington D.C., 1995.

[94] H.C. Helgeson, J.M. Delany, H.W. Nesbitt, Summary and critique of the thermodynamic properties of rock-forming minerals, Am. J. Sci., 278-A (1978).

[95] M.W. Chase, Jr., NIST-JANAF Thermochemical Tables, Fourth Edition, J. Phys. Chem. Ref. Data, 4th Ed., 1998.

[96] D.D. Wagman, W.H. Evans, V.B. Parker, R.H. Schumm, I. Halow, The NBS tables of chemical thermodynamic properties: selected values for inorganic and $C_1$ and $C_2$ organic substances in SI units, American Chemical Society and the American Institute of Physics for the National Bureau of Standards, New York, 1982.

[97] E.L. Shock, D.C. Sassani, M. Willis, D.A. Sverjensky, Inorganic species in geologic fluids: correlations among standard molal thermodynamic properties of aqueous ions and hydroxide complexes, Geochim. Cosmochim. Acta, 61 (1997) 907-950.

[98] D.A. Sverjensky, E.L. Shock, H.C. Helgeson, Prediction of the thermodynamic properties of aqueous metal complexes to 1000°C and 5 kb, Geochim. Cosmochim. Acta, 61 (1997) 1359-1412.

[99] E.L. Shock, H.C. Helgeson, D.A. Sverjensky, Calculation of the thermodynamic and transport properties of aqueous species at high pressures and temperatures: standard partial molal properties of inorganic neutral species, Geochim. Cosmochim. Acta, 53 (1989) 2157-2183.

[100] J.W. Johnson, E.H. Oelkers, H.C. Helgeson, SUPCRT92: A software package for calculating the standard molal thermodynamic properties of minerals, gases, aqueous species, and reactions from 1 to 5000 bar and 0 to 1000°C, Comput. Geosci., 18 (1992) 899-947.

[101] B. Lothenbach, L. Pelletier-Chaignat, F. Winnefeld, Stability in the system $CaO–Al_2O_3–H_2O$, Cem. Concr. Res., 42 (2012) 1621-1634.

# Appendix A. Additional details of the C-(N-)A-S-H sublattice solid solution model

Derivation of the C-(N-)A-S-H thermodynamic model begins by rearranging the SGM (eq.(A1), [38]) into an alternative structural form:

$$Ca_X H_{(6n-2X)} \left( Si_{(1-a_0)} R_{a_0} \right)_{(3n-1)} O_{(9n-2)} \cdot l^{c+}_{\frac{a_0}{c}(3n-1)} \cdot zCa(OH)_2 \cdot mH_2O \quad \text{(A26)}$$

where $R$ is a trivalent cation in tetrahedral coordination (e.g. $Al^{3+}$), $l$ is a charge-balancing interlayer cation (such as $Ca^{2+}$) with a positive charge of $c$, $m$ defines the amount of bound interlayer water, $n$ is the number of dreierketten units per non-crosslinked C-(N-)A-S-H chain, $a_0$ is the extent of substitution in aluminosilicate chains and the parameters $X$, $z$, $a_0$ and $n$ are defined according to eq.(A2):

$$\left.\begin{aligned} X &= 0.5(6n - w) \\ z &= 0.5\left[ w + n(y - 2) \right] \\ 0 \le a_0 &\le \frac{n-1}{(3n-1)} \end{aligned}\right\} \quad \text{(A27)}$$

The parameters $w$ and $y$ are related to the extent of protonation of chain tetrahedra and amount of solid solution $Ca(OH)_2$ present in the gel. Rearrangement of the SGM begins by normalising eq.(A1) to a basis of one dreierketten unit by dividing by $n$, expressed in terms of $w$ and $n$ for $X$ and $z$, and then simplified to obtain eq.(A3):

$$Ca_{\left(3-\frac{w}{2n}\right)} H_{\left(\frac{w}{n}\right)} O_{\left(9-\frac{2}{n}\right)} \cdot \left( Si_{(1-a_0)} R_{a_0} \right)_{\left(3-\left(\frac{1}{n}\right)\right)} \cdot l^{c+}_{\frac{a_0}{c}\left(3-\frac{1}{n}\right)} \cdot \left( \frac{w}{2n} - \frac{y}{2} - 1 \right) Ca(OH)_2 \cdot \left( \frac{m}{n} \right) H_2O \quad \text{(A28)}$$

The following notation is now introduced into eq.(A3): $v = 1/n$ ($0 \le v \le 1$), defines the ratio of chains per dreierketten unit, which is a measure of the number of vacant bridging tetrahedra; $u = w/n$, the

content of chemically incorporated (hydroxyl) water per dreierketten unit; and $h = m/n$, the bound water content. The introduction of this notation results in eq.(A4):

$$Ca_{\left(3-\frac{u}{2}\right)}H_uO_{(9-2\nu)}\cdot\left(Si_{(1-a_0)}R_{a_0}\right)_{(3-\nu)}\cdot l^{c+}_{\frac{a_0}{c}(3-\nu)}\cdot\left(\frac{u}{2}-\frac{y}{2}-1\right)Ca\left(OH\right)_2\cdot hH_2O \qquad \text{(A29)}$$

Eq.(A4) is then re-written to isolate two distinct sublattice sites within the chain structure, being a 'main chain dreierketten unit' ($TU$) and a 'bridging tetrahedral unit' ($BT$). This leads to a subtle change in the substitution parameter, $a_0$, which is now written as $a$, the extent of substitution in bridging sites. The resulting equation is:

$$\left[Ca\left(OH\right)_2\right]_{\left(\frac{u+y-2}{2}\right)}\cdot\left[\left(CaSiO_{3.5}\right)_2^-\right]\cdot\left[\left(Si_{(1-a)}R_aO_2\right)_{(1-\nu)}\right]^{a(1-\nu)-}\cdot\left[\left(l^{c+}_{\frac{a}{c}(1-\nu)}\right)\right]^{a(1-\nu)+}\cdot\left[Ca_{\left(1-\frac{u}{2}\right)}H_u\right]^{2+}\cdot hH_2O \qquad \text{(A30)}$$

Eq.(A5) is equivalent to eq.(2) in the main body of the text.

# Appendix B. Activity coefficient relationships for the C-(N-)A-S-H end-members

The relationships for the fictive activity coefficients for the end-members of the C-(N-)A-S-H sublattice solid solution model are defined here in terms of the following notation: 5CA = 0, INFCA = 1, 5CNA = 2, INFCNA = 3, INFCN = 4, T2C* = 5, T5C* = 6, TobH* = 7.

$$\ln(\lambda_0) = 2\ln(\chi_0+\chi_1)+2\ln(\chi_0+\chi_1)+2\ln(\chi_0+\chi_2+\chi_5+\chi_6)+ \ln(\chi_0+\chi_5+\chi_6)+\ln(\chi_0+\chi_5+\chi_6)+\ln(\chi_0+\chi_1+\chi_2+\chi_3+\chi_4)-\ln(\chi_0) \quad \text{(B31)}$$

$$\ln(\lambda_1) = 2\ln(\chi_0+\chi_1)+2\ln(\chi_0+\chi_1)+2\ln(\chi_1+\chi_4+\chi_7)+ \ln(\chi_1)+\ln(\chi_1+\chi_4+\chi_7)+\ln(\chi_0+\chi_1+\chi_2+\chi_3+\chi_4)-\ln(\chi_1) \quad \text{(B32)}$$

$$\ln(\lambda_2) = 2\ln(\chi_2+\chi_3)+2\ln(\chi_2+\chi_3)+2\ln(\chi_0+\chi_2+\chi_5+\chi_6)+ \ln(\chi_2)+\ln(\chi_2)+\ln(\chi_0+\chi_1+\chi_2+\chi_3+\chi_4)-\ln(\chi_2) \quad \text{(B33)}$$

$$\ln(\lambda_3) = 2\ln(\chi_2+\chi_3)+2\ln(\chi_2+\chi_3)+2\ln(\chi_3)+ \ln(\chi_3)+\ln(\chi_3)+\ln(\chi_0+\chi_1+\chi_2+\chi_3+\chi_4)-\ln(\chi_3) \quad \text{(B34)}$$

$$\ln(\lambda_4) = 2\ln(\chi_4)+2\ln(\chi_4)+2\ln(\chi_1+\chi_4+\chi_7)+ \ln(\chi_4)+\ln(\chi_1+\chi_4+\chi_7)+\ln(\chi_0+\chi_1+\chi_2+\chi_3+\chi_4)-\ln(\chi_4) \quad \text{(B35)}$$

$$\ln(\lambda_5) = 2\ln(\chi_5)+2\ln(\chi_5)+2\ln(\chi_0+\chi_2+\chi_5+\chi_6)+ \ln(\chi_0+\chi_5+\chi_6)+\ln(\chi_0+\chi_5+\chi_6)+\ln(\chi_5+\chi_6+\chi_7)-\ln(\chi_5) \quad \text{(B36)}$$

$$\ln(\lambda_6) = 2\ln(\chi_6+\chi_7)+2\ln(\chi_6+\chi_7)+2\ln(\chi_0+\chi_2+\chi_5+\chi_6)+ \ln(\chi_0+\chi_5+\chi_6)+\ln(\chi_0+\chi_5+\chi_6)+\ln(\chi_5+\chi_6+\chi_7)-\ln(\chi_6) \quad \text{(B37)}$$

$$\ln(\lambda_7) = 2\ln(\chi_6+\chi_7)+2\ln(\chi_6+\chi_7)+2\ln(\chi_1+\chi_4+\chi_7)+ \ln(\chi_7)+\ln(\chi_1+\chi_4+\chi_7)+\ln(\chi_5+\chi_6+\chi_7)-\ln(\chi_7) \quad \text{(B38)}$$

# Appendix C. Thermodynamic properties of the constituent phases and the relevant phases for thermodynamic modelling in this work

The solid constituents used in the additivity method and eq.(23), to estimate the standard absolute isobaric heat capacity and absolute entropy at standard state of the C-(N-)A-S-H end-members, are shown in Table C1. The gases, aqueous species and solid phases used in the thermodynamic modelling simulations are shown in Tables C2-C4.

Table C1. Thermodynamic properties of the solid constituents used to estimate $Cp^o$ and $S^o$ for the C-(N-)A-S-H end-members. The reference state is 298.15 K and 1 bar.

| Phase | $V°$ ($cm^3$/mol) | $\Delta_f H°$ (kJ/mol) | $\Delta_f G°$ (kJ/mol) | $S°$ (J/mol.K) | $Cp°$ (J/mol.K) | Reference |
|---|---|---|---|---|---|---|
| Portlandite, $Ca(OH)_2$ | 33.1 | -984.7 | -897.0 | 83.4 | 87.5 | [93] |
| Amorphous $SiO_2$ | 29.0 | -903.3 | -848.9 | 41.3 | 44.5 | [17, 94] |
| Gibbsite, $Al(OH)_3$ | 32.0 | -1289 | -1151 | 70.1 | 93.1 | [94] |
| $NaOH_{(s)}$ | 18.8 | -425.8 | -379.6 | 64.4 | 59.5 | [93, 95] |
| T2C, $(CaO)_{1.5}(SiO_2)_1(H_2O)_{2.5}$ | 80.6 | -2722 | -2467 | 167 | 237 | [25] |

**Table C2.** Thermodynamic properties of the gases used in the thermodynamic modelling simulations. The reference state is 298.15 K and 1 bar.

| Gas | $V°$ ($cm^3$/mol) | $\Delta_f H°$ (kJ/mol) | $\Delta_f G°$ (kJ/mol.K) | $S°$ (J/mol.K) | $Cp°$ (J/mol.K) | Reference |
|---|---|---|---|---|---|---|
| $N_2$ | 24790 | 0 | 0 | 191.6 | 29.1 | [96] |
| $O_2$ | 24790 | 0 | 0 | 205.1 | 29.3 | [96] |
| $H_2$ | 24790 | 0 | 0 | 130.7 | 28.8 | [96] |

**Table C3.** Thermodynamic properties of the aqueous species used in the thermodynamic modelling simulations. The reference state is unit activity in a hypothetical one molal solution referenced to infinite dilution at any temperature and pressure for aqueous species [70].

| Species | $V°$ ($cm^3$/mol) | $\Delta_f H°$ (kJ/mol) | $\Delta_f G°$ (kJ/mol.K) | $S°$ (J/mol.K) | $Cp°$ (J/mol.K) | Reference |
|---|---|---|---|---|---|---|
| $Al^{3+}$ | -45.2 | -530.6 | -483.7 | -325.1 | -128.7 | [97] |
| $AlO^+$ (+ $H_2O$ = $Al(OH)_2^+$) | 0.3 | -713.6 | -660.4 | -113 | -125.1 | [97] |
| $AlO_2^-$ (+ $2H_2O$ = $Al(OH)_4^-$) | 9.5 | -925.6 | -827.5 | -30.2 | -49 | [97] |
| $AlOOH^o$ (+ $2H_2O$ = $Al(OH)_3^o$) | 13 | -947.1 | -864.3 | 20.9 | -209.2 | [97] |
| $AlOH^{2+}$ | -2.7 | -767.3 | -692.6 | -184.9 | 56 | [97] |
| $AlHSiO_3^{2+}$ (+ $H_2O$ = $AlSiO(OH)_3^{2+}$) | -40.7 | -1718 | -1541 | -304.2 | -215.9 | [64] |
| $AlSiO_4^-$ (+ $3H_2O$ = $AlSiO(OH)_6^-$) | 25.5 | -1834 | -1681 | 11.1 | -4.6 | [64] |
| $AlSO_4^+$ | -6.0 | -1423 | -1250 | -172.4 | -204.0 | [64] |
| $Al(SO_4)_2^-$ | 31.1 | -2338 | -2006 | -135.5 | -268.4 | [64] |
| $Ca^{2+}$ | -18.4 | -543.1 | -552.8 | -56.5 | -30.9 | [97] |
| $CaOH^+$ | 5.8 | -751.6 | -717 | 28 | 6 | [97] |
| $Ca(HSiO_3)^+$ (+ $H_2O$ = $CaSiO(OH)_3^+$) | -6.7 | -1687 | -1574 | -8.3 | 137.8 | [98] |
| $CaSiO_3^o$ (+ $H_2O$ = $CaSiO_2(OH)_2^o$) | 15.7 | -1668 | -1518 | -136.7 | 88.9 | [64] |
| $CaSO_4^o$ | 4.7 | -1448 | -1310 | 20.9 | -104.6 | [98] |
| $K^+$ | 9.0 | -252.1 | -282.5 | 101 | 8.4 | [97] |
| $KOH^o$ | 15 | -474.1 | -437.1 | 108.4 | -85 | [97] |
| $KSO_4^-$ | 27.5 | -1159 | -1032 | 146.4 | -45.1 | [98] |
| $Na^+$ | -1.2 | -240.3 | -261.9 | 58.4 | 38.1 | [97] |
| $NaOH^o$ | 3.5 | -470.1 | -418.1 | 44.8 | -13.4 | [97] |
| $NaSO_4^-$ | 18.6 | -1147 | -1010 | 101.8 | -30.1 | [64] |
| $HSiO_3^-$ (+ $H_2O$ = $SiO(OH)_3^-$) | 4.5 | -1145 | -1014 | 20.9 | -87.2 | [98] |
| $SiO_2^o$ | 16.1 | -887.9 | -833.4 | 41.3 | 44.5 | [17, 99] |
| $SiO_3^{2-}$ (+ $H_2O$ = $SiO_2(OH)_2^{2-}$) | 34.1 | -1099 | -938.5 | -80.2 | 119.8 | [64] |
| $S_2O_3^{2-}$ | 27.6 | -649.9 | -520.0 | 66.9 | -238.5 | [97] |
| $HSO_3^-$ | 33.0 | -627.7 | -529.1 | 139.7 | -5.4 | [97] |
| $SO_3^{2-}$ | -4.1 | -636.9 | -487.9 | -29.3 | -281.0 | [97] |
| $HSO_4^-$ | 34.8 | -889.2 | -755.8 | 125.5 | 22.7 | [97] |
| $SO_4^{2-}$ | 12.9 | -909.7 | -744.5 | 18.8 | -266.1 | [97] |
| $H_2S^o$ | 35.0 | -39.0 | -27.9 | 125.5 | 179.2 | [99] |
| $HS^-$ | 20.2 | -16.2 | 12.0 | 68.2 | -93.9 | [97] |
| $S^{2-}$ | 20.2 | 92.2 | 120.4 | 68.2 | -93.9 | [63] |
| $Mg^{2+}$ | -22.0 | -465.9 | -454.0 | -138.1 | -21.7 | [97] |
| $MgOH^+$ | 1.6 | -690.0 | -625.9 | -79.9 | 129.2 | [97] |
| $MgHSiO_3^+$ (+ $H_2O$ = $MgSiO(OH)_3^+$) | -10.9 | -1614 | -1477 | -99.5 | 158.6 | [97] |
| $MgSO_4^o$ | 1.8 | -1369 | -1212 | -50.9 | -90.3 | [63, 97] |
| $MgSiO_3^o$ (+ $H_2O$ = $MgSiO_2(OH)_2^o$) | 12.1 | -1597 | -1425 | -218.3 | 98.2 | [63] |
| $OH^-$ | -4.7 | -230 | -157.3 | -10.7 | -136.3 | [97] |
| $H^+$ | 0 | 0 | 0 | 0 | 0 | [97] |
| $H_2O^o$ | 18.1 | -285.9 | -237.2 | 69.9 | 75.4 | [100] |
| $N_2^o$ | 33.4 | -10.4 | 18.2 | 95.8 | 234.2 | [99] |
| $O_2^o$ | 30.5 | -12.2 | 16.4 | 109 | 234.1 | [99] |

**Table C4.** Thermodynamic properties of the solid phases used in the thermodynamic modelling simulations. The reference state is 298.15 K and 1 bar.

| Phase | $V°$ ($cm^3$/mol) | $\Delta_f H°$ (kJ/mol) | $\Delta_f G°$ (kJ/mol.K) | $S°$ (J/mol.K) | $Cp°$ (J/mol.K) | Reference |
|---|---|---|---|---|---|---|
| $Al(OH)_3$ (microcrystalline) | 32.0 | -1265 | -1148 | 140 | 93.1 | [101] |
| Portlandite, $Ca(OH)_2$ | 33.1 | -984.7 | -897 | 83.4 | 87.5 | [93] |
| Amorphous $SiO_2$ | 29.0 | -903.3 | -849 | 41.3 | 44.5 | [17, 94] |
| $C_2AH_8$ | 90.1 | -5278 | -4696 | 450 | 521 | [101] |
| $C_3AH_6$ | 150 | -5537 | -5008 | 422 | 446 | [101] |
| $C_4AH_{13}$ | 27.4 | -8302 | -7327 | 700 | 930 | [66] |
| $C_4AH_{19}$ | 382 | -1002 | -8750 | 1120 | 1382 | [101] |
| $C_4AH_{10}$ | 194 | -5388 | -4623 | 610 | 668 | [101] |
| Monosulfate, $C_4AsH_{12}$ | 309 | -8750 | -7779 | 821 | 942 | [64] |
| Stratlingite, $C_2ASH_8$ | 21.6 | -6360 | -5705 | 546 | 603 | [64] |
| Ettringite, $C_6As_3H_{32}$ | 707 | -17535 | -15206 | 1900 | 2174 | [66] |
| Hydrotalcite, $M_4AH_{10}$ | 220 | -7196 | -6395 | 549 | 649 | [66] |
| Brucite, $Mg(OH)_2$ | 24.6 | -923 | -832 | 63.1 | 77.3 | [94] |
| **The 'downscaled CSH3T' model [a]** | | | | | | |
| TobH, $(CaO)_1(SiO_2)_{1.5}(H_2O)_{2.5}$ | 85.0 | -2833 | -2562 | 153 | 231 | [25] |
| T5C, $(CaO)_{1.25}(SiO_2)_{1.25}(H_2O)_{2.5}$ | 79.3 | -2782 | -2519 | 160 | 234 | [25] |
| T2C, $(CaO)_{1.5}(SiO_2)_1(H_2O)_{2.5}$ | 80.6 | -2722 | -2467 | 167 | 237 | [25] |

[a] The mixing rules used to describe the downscaled CSH3T model and the thermodynamic properties that define the TobH, T5C and T2C end-members in GEM-Selektor are the same as those described in [25] for this model. The Gibbs free energies (and thus the enthalpies) of these components are modified slightly to the corresponding values used to define the TobH*, T5C* and T2C* end-members of the CNASH_ss model (Table 2).

# Appendix D. Additional simulation results used to validate the thermodynamic model

Additional simulation results that were used to validate the thermodynamic model are shown in Figures D1-D6.

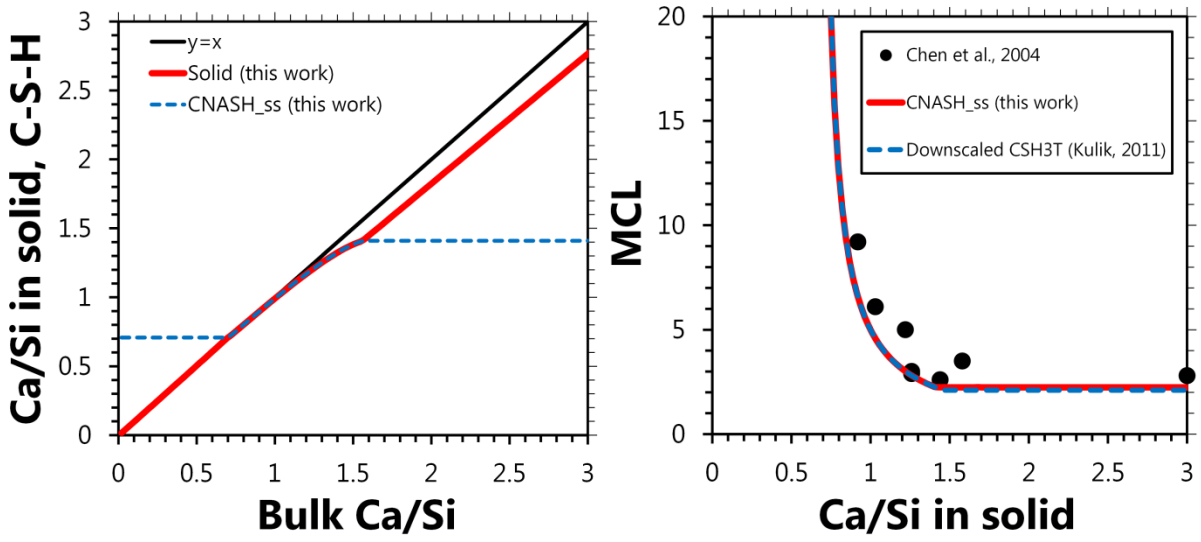


**Figure D1**. Simulation results (25°C, 1 bar, 0.25 M NaOH/solids mass ratio = 50) using the thermodynamic model developed here (CNASH_ss) in addition to those presented in Figure 2. The MCL calculations are compared to the data reported in [8] and the simulation results using the downscaled CSH3T model [25]. The thermodynamic properties of the phases included in these simulations are given in Appendix C.

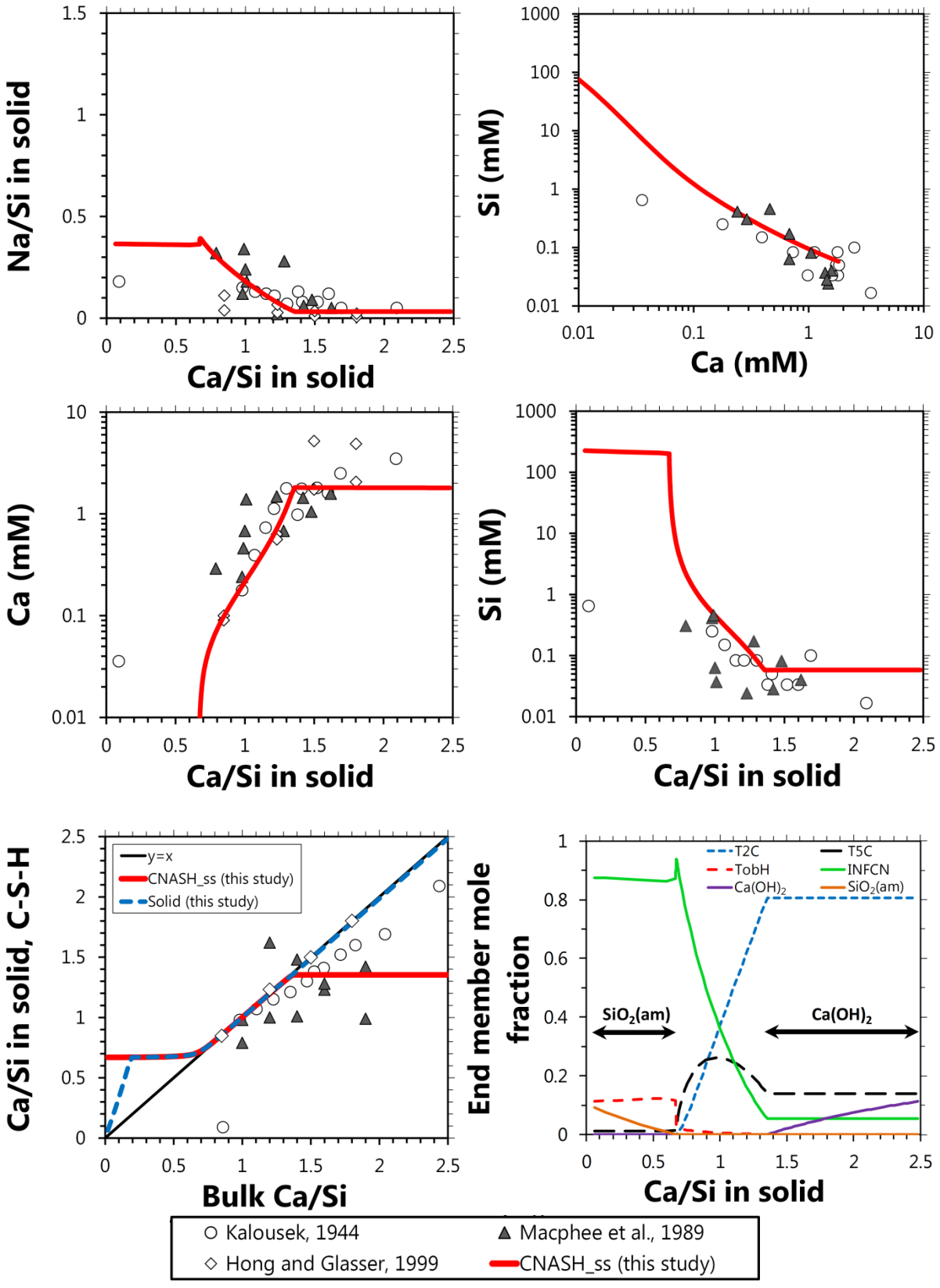


**Figure D2**. Comparison of the simulation results (25°C, 1 bar, 0.25 M NaOH/solids mass ratio = 50) using the thermodynamic model developed here (CNASH_ss, bold red traces) to published solubility data in the CaO-$Na_2O$-$SiO_2$-$H_2O$ system at alkali concentrations 0.1 M ≤ [NaOH] ≤ 0.3 M [76, 80, 81]. The thermodynamic properties of the phases included in these simulations are given in Appendix C.

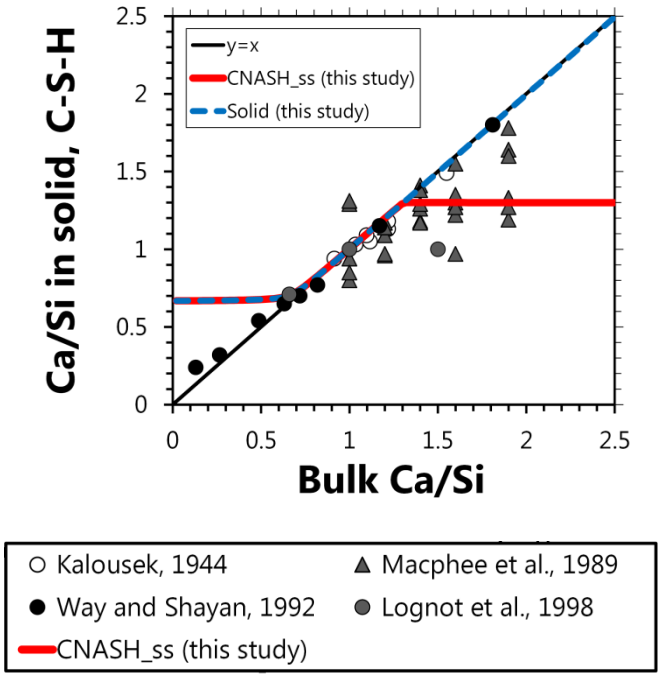


**Figure D3**. Comparison of the simulation results (25°C, 1 bar, 0.5 M NaOH/solids mass ratio = 50) using the thermodynamic model developed here (CNASH_ss, bold red traces) to solid chemistry data in the $CaO$-$Na_2O$-$SiO_2$-$H_2O$ system at alkali concentrations 0.3 M ≤ [NaOH] ≤ 0.8 M [76, 80, 81], in addition to the results shown in Figure 3 for this system. The thermodynamic properties of the phases included in these simulations are given in Appendix C.

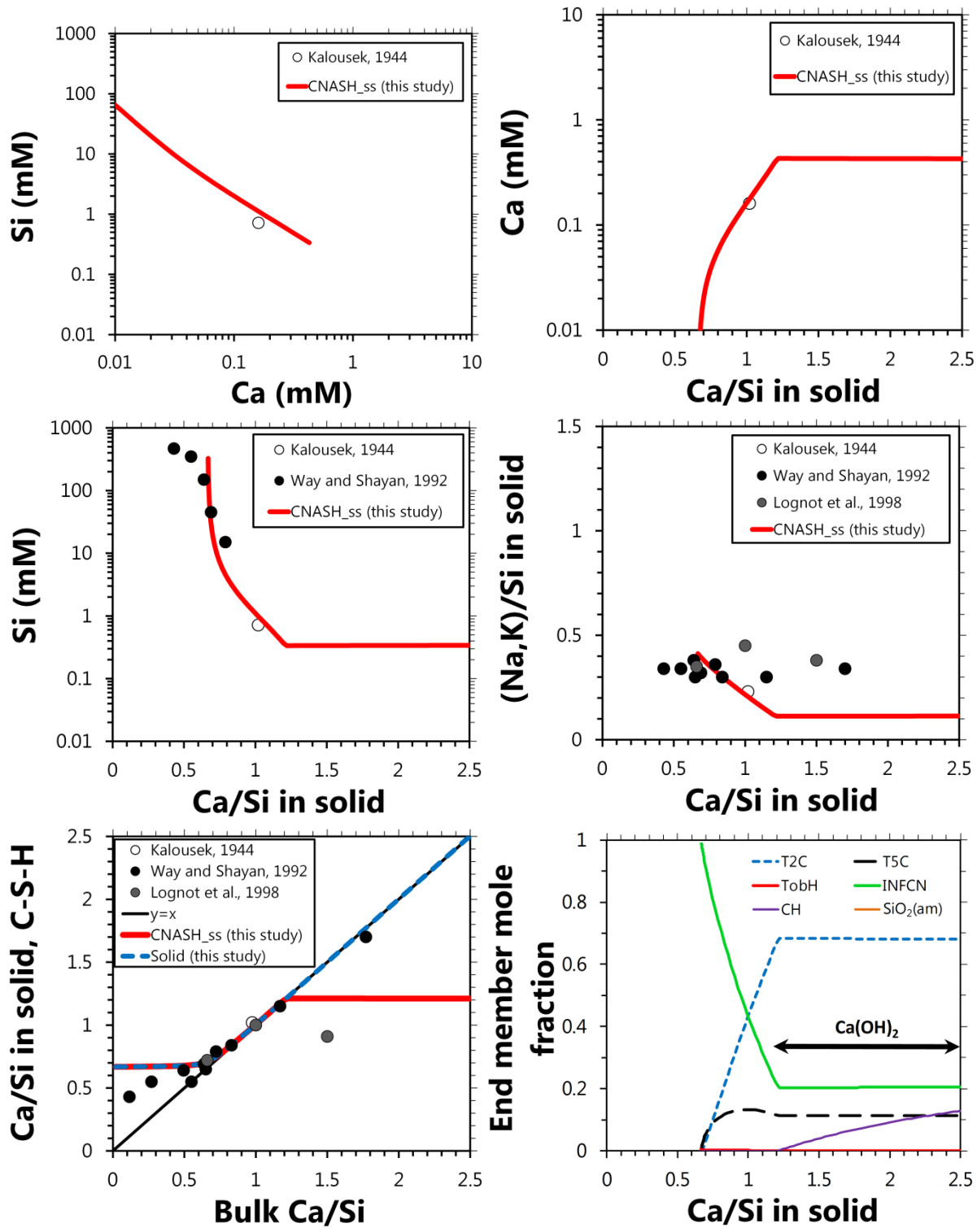


**Figure D4**. Comparison of the simulation results (25°C, 1 bar, 1 M NaOH/solids mass ratio = 50) using the thermodynamic model developed here (CNASH_ss, bold red traces) to solubility and solid phase chemistry data in the CaO-$Na_2O$-$SiO_2$-$H_2O$ system at alkali concentrations 0.8 M ≤ [NaOH] ≤ 1 M [75, 77, 80]. The corresponding end member mole fraction results are also shown. The thermodynamic properties of the phases included in these simulations are given in Appendix C.

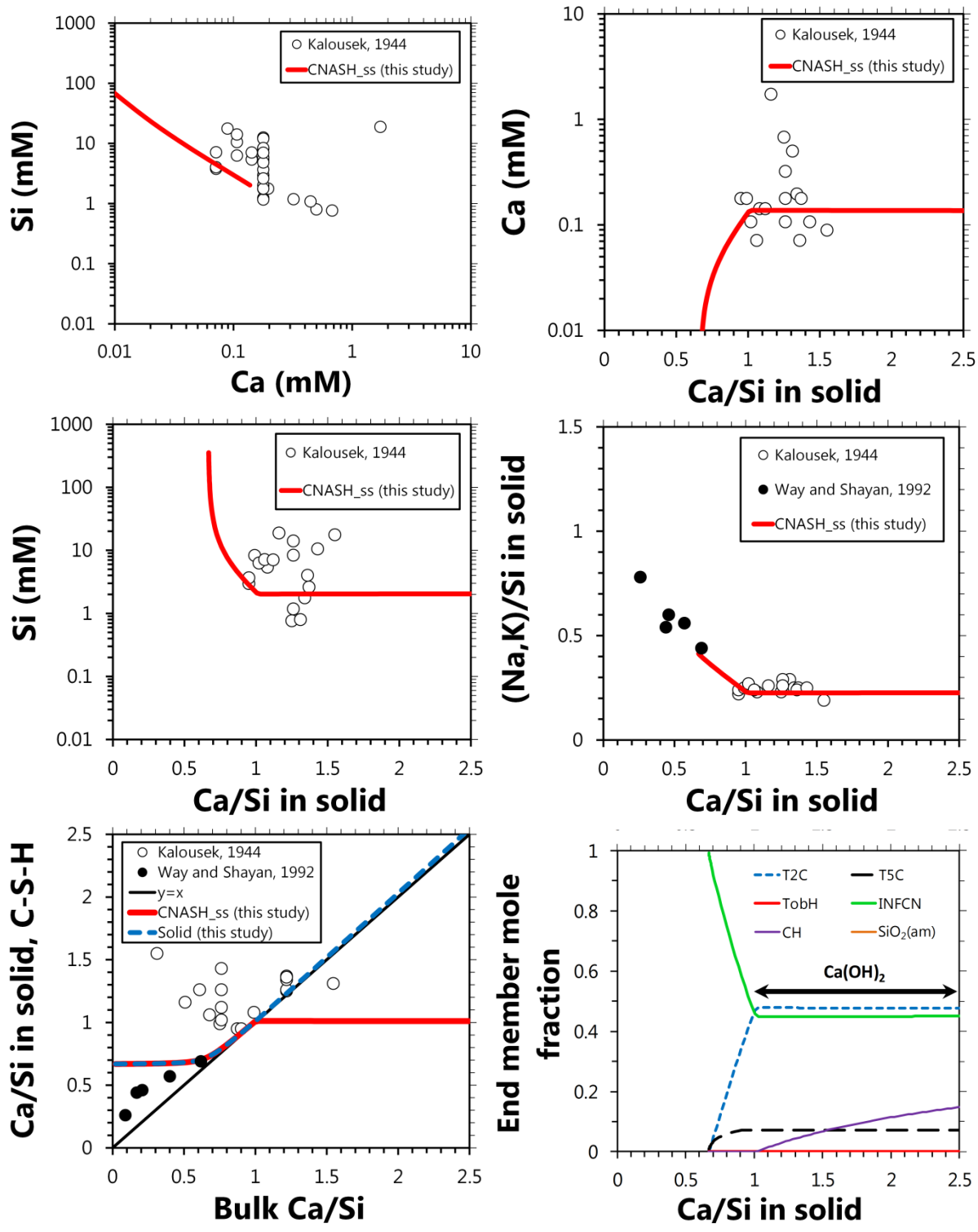


**Figure D5**. Comparison of the simulation results (25°C, 1 bar, 3 M NaOH/solids mass ratio = 50) using the thermodynamic model developed here (CNASH_ss, bold red traces) to solubility and solid phase chemistry data in the CaO-$Na_2O$-$SiO_2$-$H_2O$ system at alkali concentrations 1 M ≤ [NaOH] ≤ 5 M [77, 80]. The corresponding end member mole fraction results are also shown. The thermodynamic properties of the phases included in these simulations are given in Appendix C.

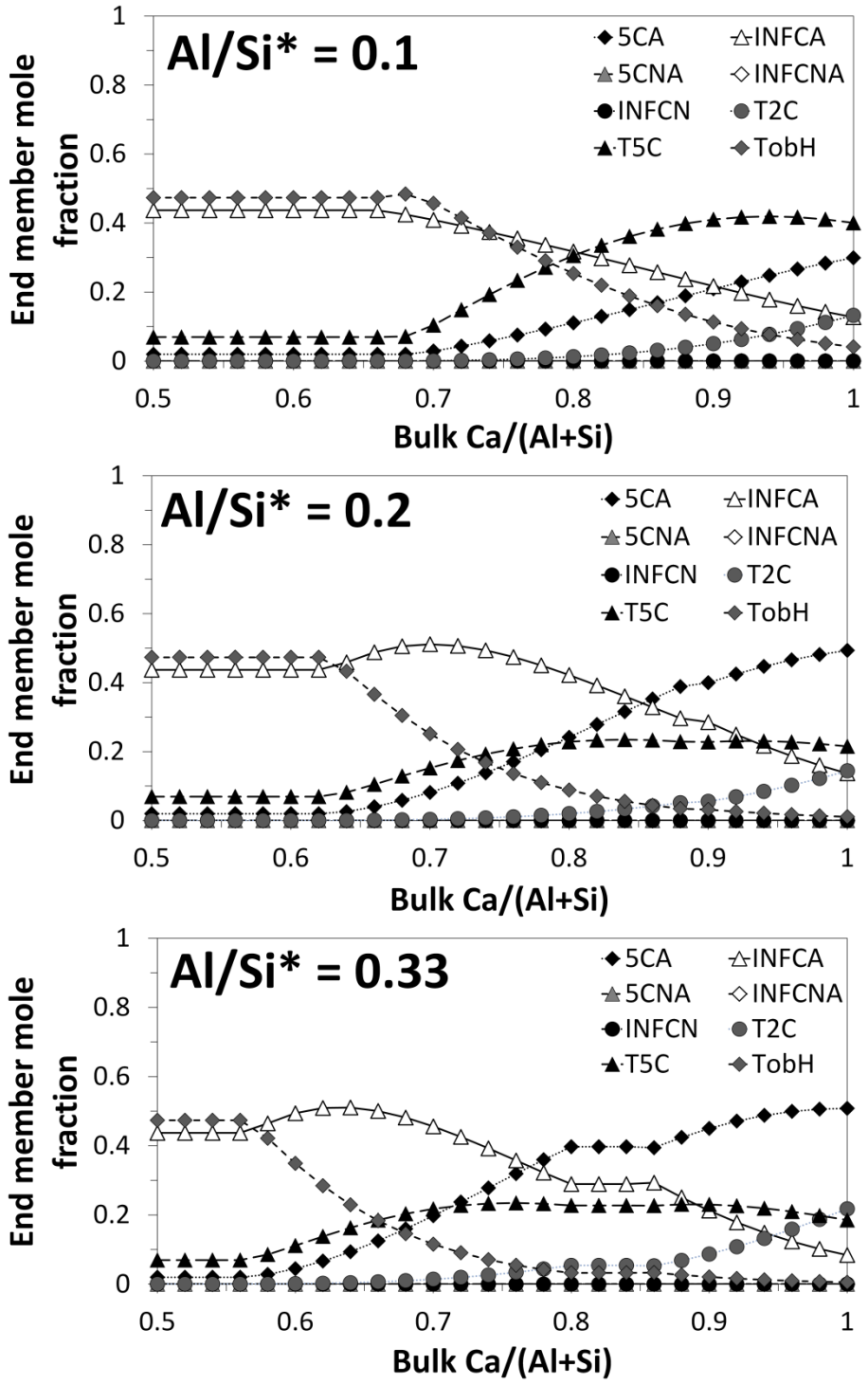


**Figure D6**. End member mole fractions corresponding to the simulation results shown in Figure 5 (25°C, 1 bar, water/solids mass ratio = 50). Al/Si* = bulk Al/Si. The thermodynamic properties of the phases included in these simulations are given in Appendix C.

# Appendix E. Additional details of the AAS cements simulated by thermodynamic modelling

The slag reaction extents, curing times and activating conditions used to simulate the pore solution chemistry of AAS cements (Figure 6) are shown in Table E1.

**Table E1**. Slag reaction extents, curing times and activating conditions used to simulate the pore solution chemistry of AAS cements.

| System (corresponding to the legend labels in Figure 6) | Curing time (days) | Activator | Water/binder | Slag reaction extent used in simulations (%) | Reference |
|---|---|---|---|---|---|
| Gruskovnjak et al., 2006 | 1 | $Na_2SiO_3.5H_2O$ | 0.3 [a] | 32 | [71] |
| Gruskovnjak et al., 2006 | 7 | $Na_2SiO_3.5H_2O$ | 0.3 [a] | 36 | [71, 87] |
| Gruskovnjak et al., 2006 | 28 | $Na_2SiO_3.5H_2O$ | 0.3 [a] | 38 | [71, 87] |
| Gruskovnjak et al., 2006 | 180 | $Na_2SiO_3.5H_2O$ | 0.3 [a] | 42 | [71, 87] |
| Puertas et al., 2004 | 7 | $Na_2O{\cdot}1.5SiO_2{\cdot}xH_2O$ | 0.5 [b] | 36 | [82] |
| Puertas et al., 2004 | 7 | NaOH | 0.5 [b] | 36 | [82] |
| Lloyd et al., 2010 | 90 | $Na_2O{\cdot}mSiO_2{\cdot}xH_2O$ | 0.35 | 40 | [83] |
| Song and Jennings, 1999 | 28 | 1 M NaOH | 0.45 [c] | 36 | [84] |
| Song and Jennings, 1999 | 28 | 0.5 M NaOH | 0.45 [c] | 31 | [84] |
| Song and Jennings, 1999 | 28 | 0.1 M NaOH | 0.45 [c] | 26 | [84] |
| Song and Jennings, 1999 | 41 | $H_2O$ | 0.45 [c] | 21 | [84] |
| Song and Jennings, 1999 | 44 | 1 M NaOH | 0.45 [c] | 39 | [84] |
| Song and Jennings, 1999 | 44 | 0.5 M NaOH | 0.45 [c] | 34 | [84] |
| Song and Jennings, 1999 | 44 | 0.1 M NaOH | 0.45 [c] | 29 | [84] |

[a] water/cement.
[b] (water + activator)/slag.
[c] liquid/slag.